4 System Characterization Experiments

A common task in system analysis is to measure the complex transfer function of a given object. It was pointed out previously that our special interest is laid on mechanical response dynamics. In case of a nanooptical system the transfer function, as we will treat it, tells us how a sinusoidal stimulus makes the object surfaces vibrate. Oscillations occur on a nanoscale. To make them visible we need a high resolution measurement equipment. Moreover if we want to resolve mechanical surface modes an accurate coordinate based navigation must be available. From the instrumentation point of view this is by far not trivial. We memorize chapter 2 : the degree of complexity, defined as the logarithmic ratio of system to minimal component or structure size, reaches up to 6 in modern nanooptics. No commercial solution is helpful here. On the one hand, the nanocartographer's AFM head is an embedded unit of the model system as declared in said chapter. On the other hand, it features the ideal built in sensing principle to characterize the system from within. Though commonly used to generate topographical images the beam deflection also allows to study periodical surface deflection at fixed coordinates. Once the cantilever is in surface contact it co-oscillates and the sensor generates an output signal proportional to the mode amplitudes. The object can be probed by single frequency or broadband stimulus. In the first case the response is often evaluated by digital lock–in amplification [ALO03], nowadays favored analysis technique in the second case is the Fast Fourier Transform (FFT) [GRUE01]. As we will feature the new ASA filter concept both in single line and broadband scenario – which are the main topics of the sections in this chapter – we can quantify the performance gain plus the improvement in quality and speed of the analysis with respect to the standards. The data gathered in the spectral response analysis proves the serviceability of the algorithms.

One has to select a test structure for these experiments. Since a piezo scanner, [VOR01] driven by a coherent electrical stimulus, develops acoustic Chladni patterns [VOG99] on the surface of its metal housing, it fulfills the criterion to have said high degree of complexity. Modes can take on lateral dimensions of several centimeters and orthonormal deformations on a nanometer scale. Since the stimulus must be ultra low to ensure linear motion [1] the quality of the system identification is highly related to the availability of disturbance and noise suppression tools. While external disturbances might be cleared using commercial vibration isolating techniques the presence of noise is unavoidable in laboratory experiments. Some noise effects can be minimized through careful experimental design (for instance electromagnetic shielding), others are of fundamental nature (shot noise, distortion in operational amplifiers, digitizing noise in analog to digital converters etc.). The working principle of the ASA filter is based on minimizing the spectral prediction error in the mean sense, so it reacts very robust on the presence of uncorrelated distortions in the sensor data. The thesis has been accompanied by a diploma works at the Institute of Applied

1 the response must not exceed 2 micron peak amplitude.

Physics, Technische Universität Darmstadt, where an algorithm for digital lock–in amplification has been developed and extensively tested in the laboratory [LEN04]. The results attained there allow for contrasting the new ASA method in phase angle and magnitude estimation. In chapter 3 we learned from theory what makes the difference between a *deterministic* and a *stochastic* solution of the identification problem. The lock–in amplifier measures the spectral line by an orthogonal projection of the the response on the reference which is truly deterministic. The ASA filter estimates it based on statistics. So now both statements are compared experimentally.

Realtime phase rectification [2] needs the provision of a reference oscillator that twiddles at the stimulation frequency. The reference either has to be created internally to the DSP (as presented in [BAR01]) or externally (as implemented here). To record resonance curves at low driving amplitudes (below 100mV) external modulation is first choice since the performance of commercial precision function generators is superior to that of the analog DSP interface [3]. In case of utilizing an external oscillator the quadrature components have to be recovered, for example by digital phase–locked–loop (PLL) synchronization. Phase fidelity of the quadrature is the key to a correct measurement of the system phasing. The tracking of reference oscillations at high dynamic bandwidth is indeed demanding. As the frequency of the driving oscillator changes rapidly a standard phase angle detector (digital charge pump model) typically generates a phase delay which results in poor response [BAN06]. One can enhance the dynamical bandwidth of the PLL by decreasing the closed loop equivalent time–constant. But that will cause the PLL to become very sensitive to harmonic disturbances and measurement noise which is unacceptable. There have been reported many studies on phase angle estimation for fast yet robust phase recovery [DJU92] [KAU97] [LEE99] [SON00] . Notably most of them can only be exploited in three–phase systems which does not comply with the resonance experiment. Sidhu and Sachdev [SID98] demonstrated an iterative technique for estimating frequency and phase in a single–phase system. Since their method is computationally demanding there is a need to reduce the effort for real time application. Fast tracking trades off for robustness against distortion. It will be demonstrated that the single line ASA filter is a most elegant alternative to the digital PLL responding roundabout 20 times faster on sudden line frequency jumps.

The multi line adaptation is explored in a DSP microcomputer simulation. The spectrum of the piezo scanner as recorded by single line frequency wobbling is used to emulate the system response on an arbitrary broadband frequency stimulus. It offers to apply frequency combs. Coherent as well as incoherent irradiation–identification scenarios are computed and compared to the results of different radix–2 FFT.

2 usual terminology for single line phase characterization

3 to compare : noise floor ADSP21160 SHARC evaluation board 40 mV
noise floor Hewlett Packard 3325A waveform generator 0.2 mV

4.1 Complex Line Tracks

We start the section with a short introduction of the experimental setup. Assume the piezo to be stimulated by a frequency generator and we want to measure the response magnitude and phase. A schematics of the experiment is shown in fig. 4.1.1.

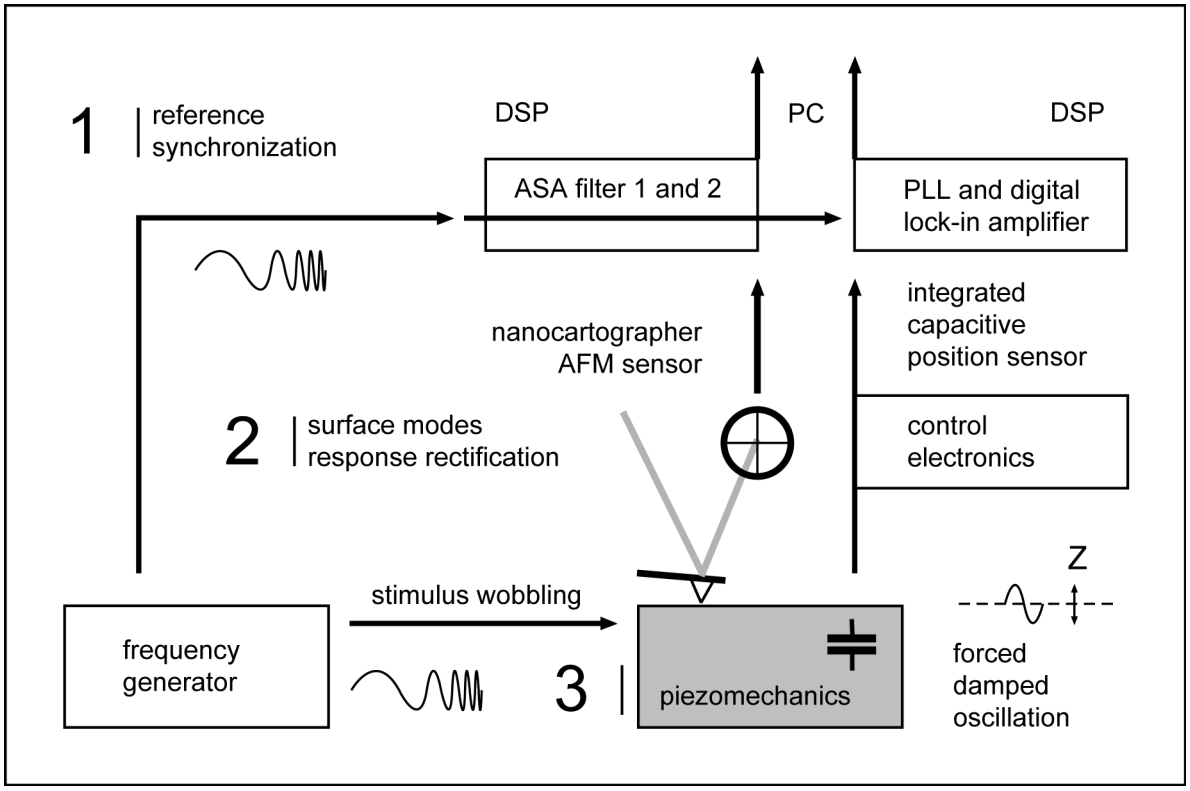

Figure 4.1.1 : *Adaptive spectrum analysis setup. The bold numbers outline the main topics of this section.*

In the first paragraph we deal with the problem of synchronizing the spectrum analysis algorithm with the external stimulus. The goal is to make a complex vector on the DSP rotate phase locked such that its real part equals the piezo driving voltage and its imaginary part is in quadrature to the output of the frequency generator. In the second paragraph we discuss the performance of the DSP software tools tracking magnitude and phase jumps in the sensor signal path. Third we measure how magnitudes propagate through the piezo mechanics. The inertia of the piezo also delays the phase relative to the synchronized reference [1] which is of particular interest. The stimulation frequency is ramped in a wobble experiment to scan the transfer function of the mechanics. Resonance curves are recorded at different coordinates on top side of the piezo stage [2], to demonstrate the advantage of the nanocartographer's navigation and cartographic resolution capabilities versus the position sensing technology integrated in the nanooptical system.

1 The reference is referred to as a numerically controlled oscillator (NCO) in DSP literature.
2 See also fig. 4.1.14 .

4.1.1 Reference Synchronization

The standard method to synchronize a numerically controlled oscillator (NCO) to a periodic signal is a phase locked loop. The function principle is illustrated in fig. 4.1.2. The phase difference between the NCO and the input signal is measured by a phase sensitive detector (PSD). The output of the PSD is lowpass filtered (LPF). The resulting phase lead or lag is used to tune the NCO frequency by a PI controller such that the phase error is minimized. The scheme applies for analog as well as digital PLLs. The challenge in PLL design is to shape the dynamics of the loop filter and the phase controller to achieve a desired response to frequency or phase steps. Details on the closed loop design can be found in the literature [BAN06].

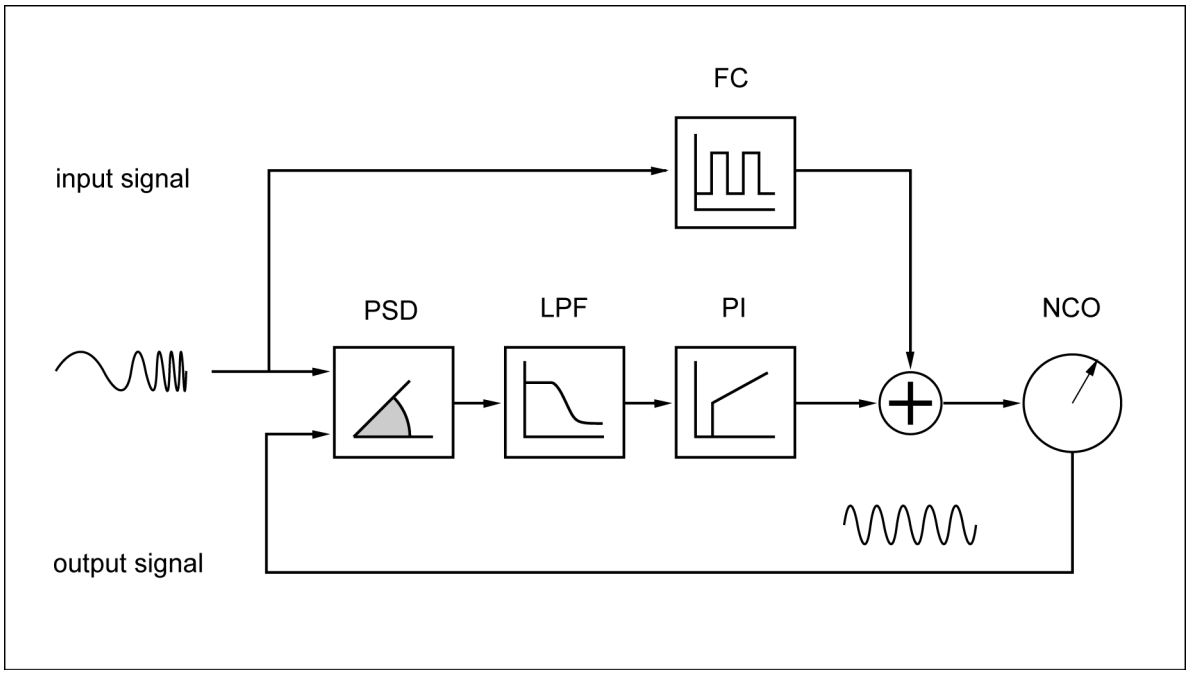

Figure 4.1.2 : *Advanced PLL assembly.*

The LPF used here is an exponential smoother [SMI99] and the digital phase controller is a PI velocity algorithm with external guide [AST02]. The exponential weight is set to 0.995. The controller is tuned for the time constant of the closed loop to approximate 100 ms. We implement the PSD according to the charge pump model – which is state of the art in analog PLL design – in a lead–lag form [ALO03]. In case of early phases it generates positive lead pulses proportional to the phase error which are averaged in the loop filter stage. Vice versa late phases changes the sign of the pulses. The pulse width modulation is depicted in fig. 4.1.3. Each time a positive slope zero crossing occurs in one of the signals the output p of the PSD alters. If the transition falls on the input, p is incremented. Otherwise it is decremented. An advanced digital PLL architecture may utilize a guided NCO frequency controller, whereas the assist is provided by an embedded frequency counter (FC). The implementation of a guide term is advantageous, since it boosts the phase lock at arbitrary frequency steps. However the FC is susceptible to spurs. Thus to minimize

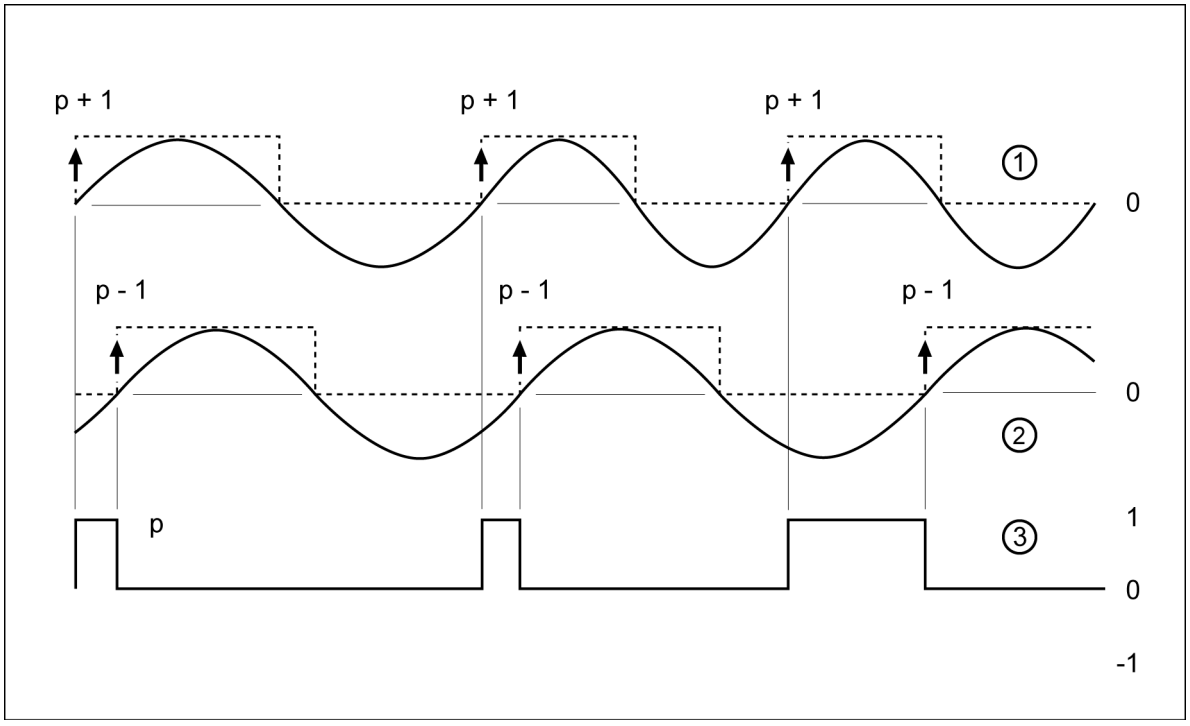

Figure 4.1.3 : *Generation of lead pulses p at the output of the phase sensitive detector. In case of a phase lag the sign of the pulses toggles.*

① PLL input signal
② NCO output signal
③ PSD output pulses

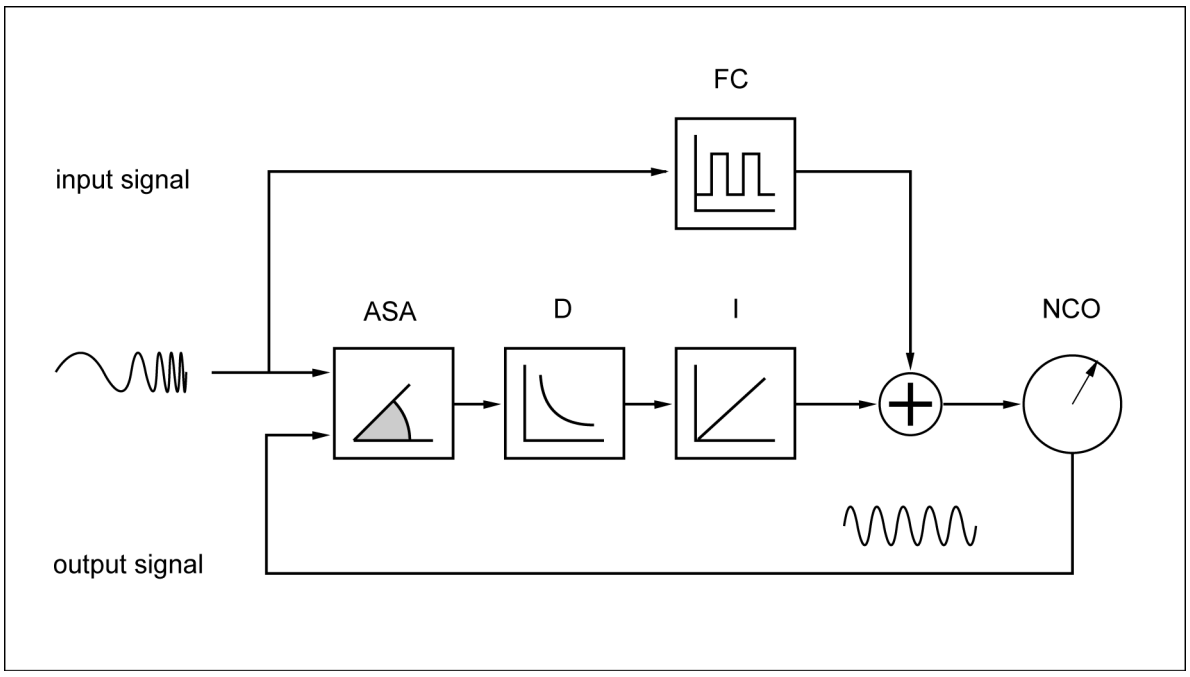

Figure 4.1.4 : *Adaptive PLL control strategy. The PSD is replaced by the single line ASA filter to generate the phase information. A differentiation of the ASA phase output measures the frequency error of the NCO. Integral action compensates for that and makes the NCO rotate at the input frequency.*

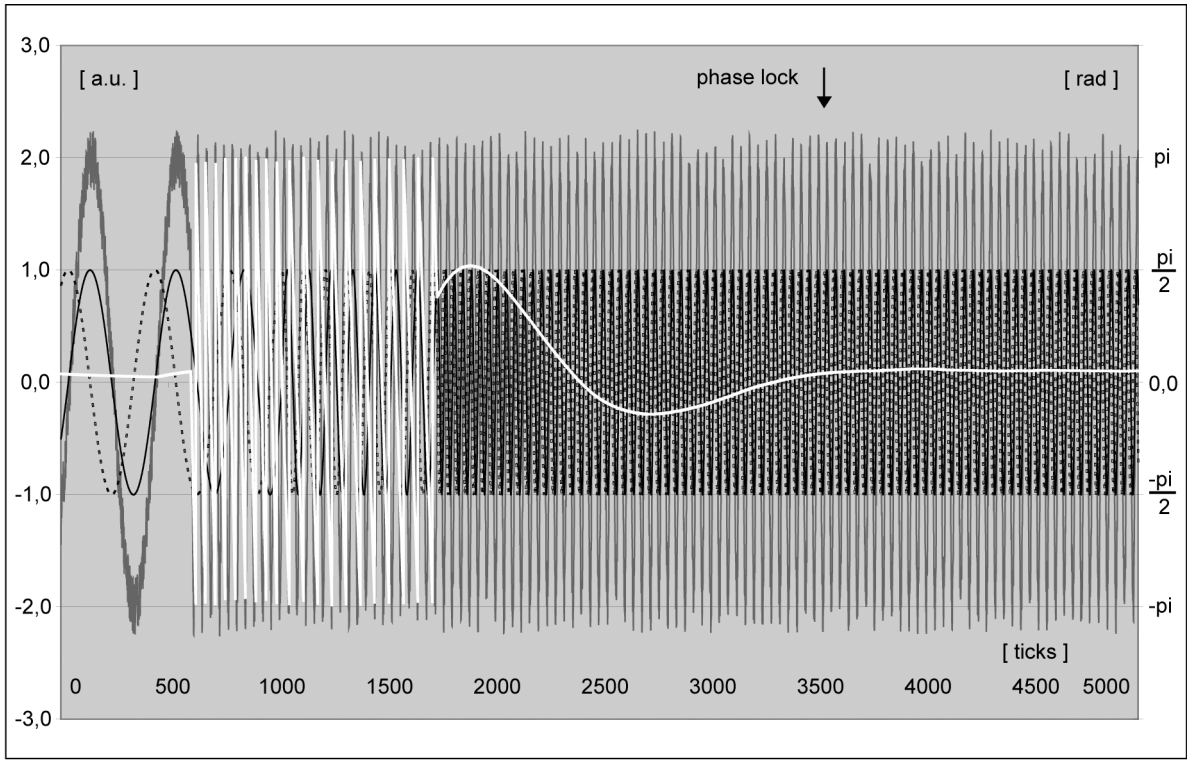

Figure 4.1.5 : *Frequency step response of the digital PLL algorithm on a jump from 50 to 500 Hz computed with an Analog Devices ADSP21160 evaluation hardware (refer to page 81).*

phase jitter the guide is discontinuously updated as the NCO frequency differs more than ± 10 percent from the guide frequency. To compare the performance of the single line ASA filter with the digital PLL we modify the phase locking strategy as shown in fig. 4.1.4. The adaptive filter measures the complex amplitude of the input signal in the rotating coordinate system of the NCO. Assume input and output frequency to be equal. In that case the spectral line is stationary. As the NCO rotates faster the adaptive filter compensates the frequency difference and it starts to turn clockwise. If we measure the phase gradient through a differential transformer D we can determine the frequency mismatch. By means of an I controller the input and output frequency can be adjusted. Notice that in steady state an arbitrary phase offset between the NCO and the input remains. But the knowledge of the complex amplitude allows to reconstruct a unity oscillator that is in zero phase delay.

Fig. 4.1.5 shows the response of the digital PLL to a frequency step from 50 to 500 Hz in a DSP experiment. The input signal, the real and the imaginary part of the NCO are plotted versus the data sampling periods whereas the sampling frequency is set to 20 kHz. The thin white line represents the phase error of the closed loop. We find the step event in the graph at tick 600. The frequency guide at that time is about 50 Hz. We register multiple phase slip errors in the following 1000 ticks. The NCO frequency slowly rises. Roughly at tick 1600 it has increased by 10 percent, thus the guide is updated by the latest frequency counter value close to 500 Hz. It takes another 2000 ticks till the phase is relocked. The NCO is unlocked for 3000 ± 300 ticks after the frequency step occurred. Ticks are synchronous to the ADC sampling.

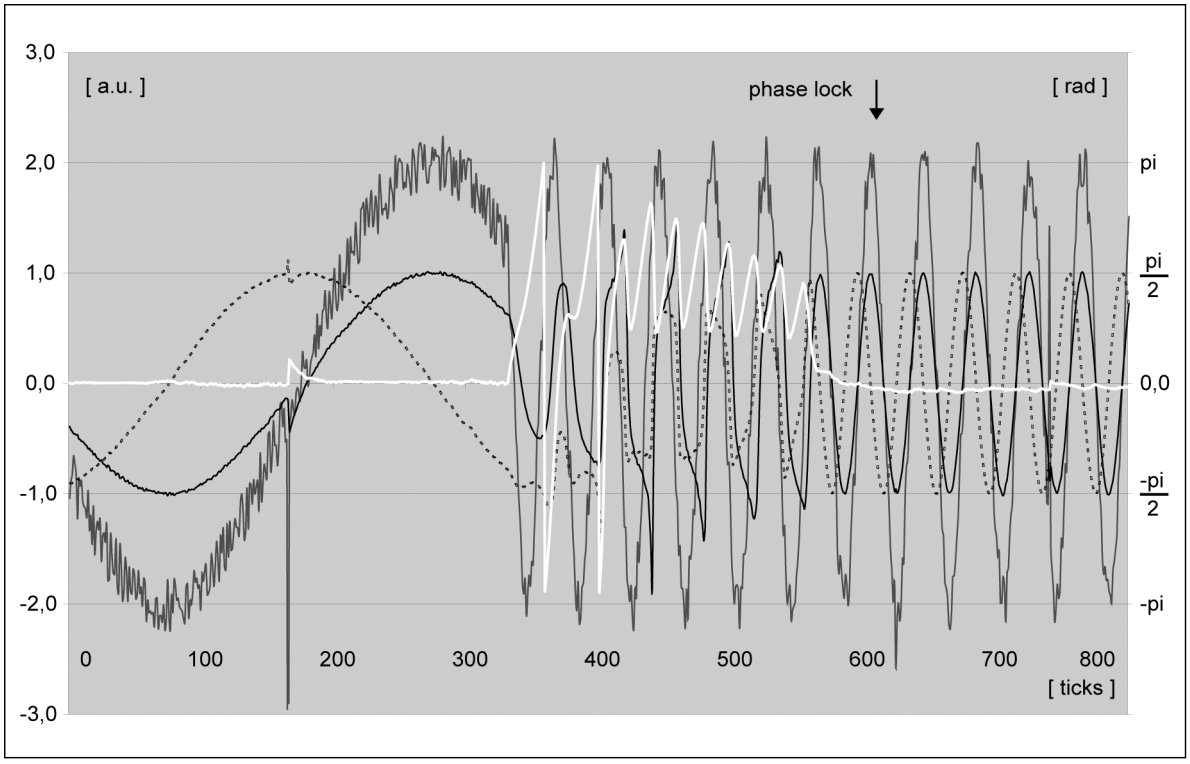

Figure 4.1.6 : *Response of the single line ASA filter on an equal frequency step.*

If we repeat the experiment with the adaptive PLL we get the data shown in fig. 4.1.6. The step event is located at tick 340. The NCO is estimated to be out of phase until tick 620. So the adaptive PLL is unlocked for 280 ± 20 ticks. This is more than 20 times faster than in the previous run.

4.1.2 Surface Modes Response Rectification

The output channels of the position sensitive devices [3] each yield a periodic signal as the surface of the piezo actuator is set into harmonic vibration. The intention is to quantify the performance gain of the ASA filter in the analysis of magnitude and phase steps at constant modulation frequency as compared to a digital lock–in amplifier. This requires normative experimental conditions. To eliminate the influence of the signal chain the sensor output is synthesized by an arbitrary waveform generator adding noise and spurs to the harmonic.

The function principle of the digital lock amplifier is depicted in fig. 4.1.7 The aim is to find the amplitude and relative phase of a system response $A \cdot \cos(\omega t + \varphi)$ with known modulation frequency f_{mod}. For that purpose the response signal is multiplied in mixer stages ⊗ with a reference sine oscillation and its quadrature cosine. The lowpass filter (LPF) reconstructs the amplitude, multiplied by a corres-

3 nanocartographer : AFM sensor piezo mechanics : integrated CAP sensor

ponding phase factor. The operation may be seen as determining the projections of the response to the oscillator base. The integration time relates to the cutoff frequency of the filter. Every lock–in amplifier contains such a phase sensitive detector (PSD).

Assume we want to detect a noise–free sinusoidal voltage given by

$$v_{in} = A\sin(\varpi t + \phi) \tag{4.1}$$

with the modulation frequency $f_{\mathrm{mod}} = \varpi / 2\pi$. The lock–in amplifier computes the orthogonal projection on a reference oscillation with equal frequency and amplitude 2. (provided internally or externally). The response signal is multiplied by the reference.

$$v_{PSD} = v_{res} \cdot v_{ref} = A\sin(\varpi t + \phi) \cdot 2\sin(\varpi t) = A\left(\cos(\phi) - \cos(2\varpi t + \phi)\right) \tag{4.2}$$

and corollary for the quadrature

$$v^{*}_{PSD} = v_{res} \cdot v_{quad} = A\sin(\varpi t + \phi) \cdot 2\cos(\varpi t) = A\left(\sin(\phi) - \sin(2\varpi t + \phi)\right) \tag{4.3}$$

The lowpass filter cuts off the ac parts, so we get at the output of the phase rectifier

$$X = A\cos(\phi) \qquad \text{and} \qquad Y = A\sin(\phi) \tag{4.4}$$

Magnitude and phase are reconstructed by

$$A = \sqrt{X^2 + Y^2} \qquad \text{and} \qquad \phi = \arctan\frac{X}{Y} \tag{4.5}$$

Now let the response signal be corrupted by additive noise. The phase sensitive rectification will block all spectral components except from the particular one lying in ϖ. Notice though the rectification can be implemented at varying reference frequencies the lowpass filter operates with a predefined magnitude profile. A second order Butterworth LPF has been selected for the experiments [LEN04]. The cutoff frequency f_c is related to the integration time T_c as

$$T_c = 1 / 2\pi f_c \tag{4.6}$$

The ASA filter tracks the quantities X and Y straight forward as discussed in chapter 3. The dimension of the NCO ensemble is 1, since we focus on a single spectral line and the filter kernel size is 2, because we track a complex quantity with real and imaginary part. We compare how the lock–in amplifier and the single line ASA filter react on sudden magnitude jumps at constant phasing. The sampling rate is set to 20 kHz and the modulation frequency is pinned at 50 Hz.

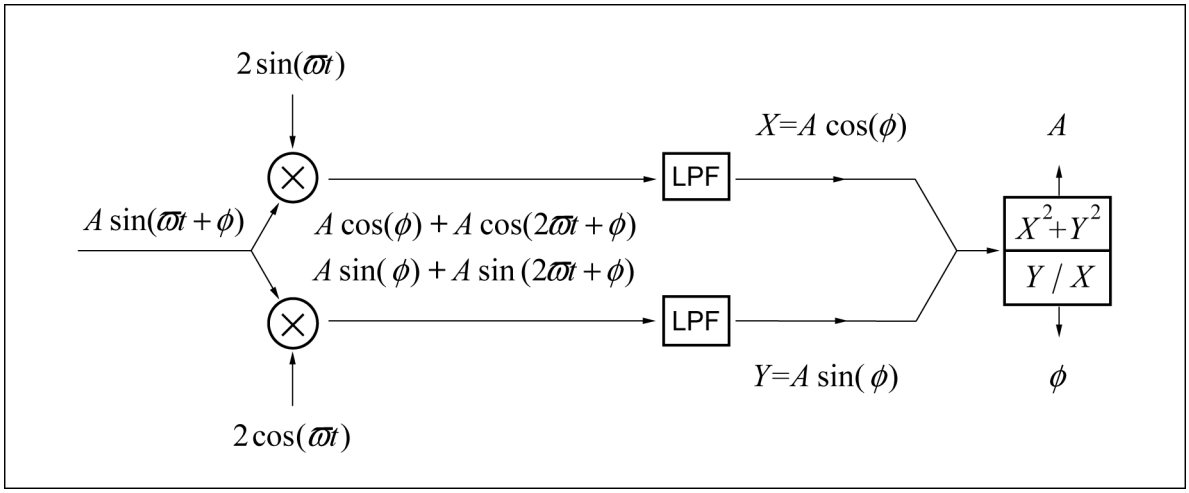

Figure 4.1.7 : *Phase rectification in a digital PSD module. The system response is projected on a reference quadrature oscillator to extract amplitude A and phase φ.*

The response of the lock–in amplifier on a step from 1 to 5 a.u. is depicted in fig. 4.1.8. An integration time of half a modulation period would be desirable [4] with respect to a fast response. But in that case the remaining ripple in the pass band is approximately 5 percent. It is known from the adaptive PLL experiment that the magnitude estimation error of the ASA filter lies close to 2 percent. Thus to gain a comparable signal to error ratio a less ambitious and longer integration time must be chosen.

The dynamics in the DSP software have been set to:

lock–in amplifier	LPF integration time	$T_c = 25\ ms$	(4.7)

and in light of the adaptive spectral analysis experiment

ASA filter [5]	measurement noise covariance	$\rho^2 = 10^{-2}$	
	system noise covariance	$\sigma^2 = 10^{-5}$	(4.8)

The identification of the spectral line with the digital lock–in amplifier has an equivalent time constant of 2000 ± 200 ticks or equivalent 100 ± 10 ms. We recognize from fig. 4.1.9 that the ASA filter is tracking much faster. When the step occurs both magnitude and phase estimation are distorted but settle quickly with equal timing. The decorrelation time is estimated from the plots as 200 ± 20 ticks or 10 ± 1 ms which equals half a modulation period. Again we find a significant improvement of the standard. We can state the ASA filter reduces the spectral estimation time by a factor of 10.

We repeat the experiment with phase steps at constant magnitude. The lock–in output is depicted in fig. 4.1.10 and the ASA filter output in fig. 4.1.11. The performance statement made for magnitudes obviously also holds for phasing. The quantities are balanced.

4 annotation : which is pretty short
5 compare table 3.1.2

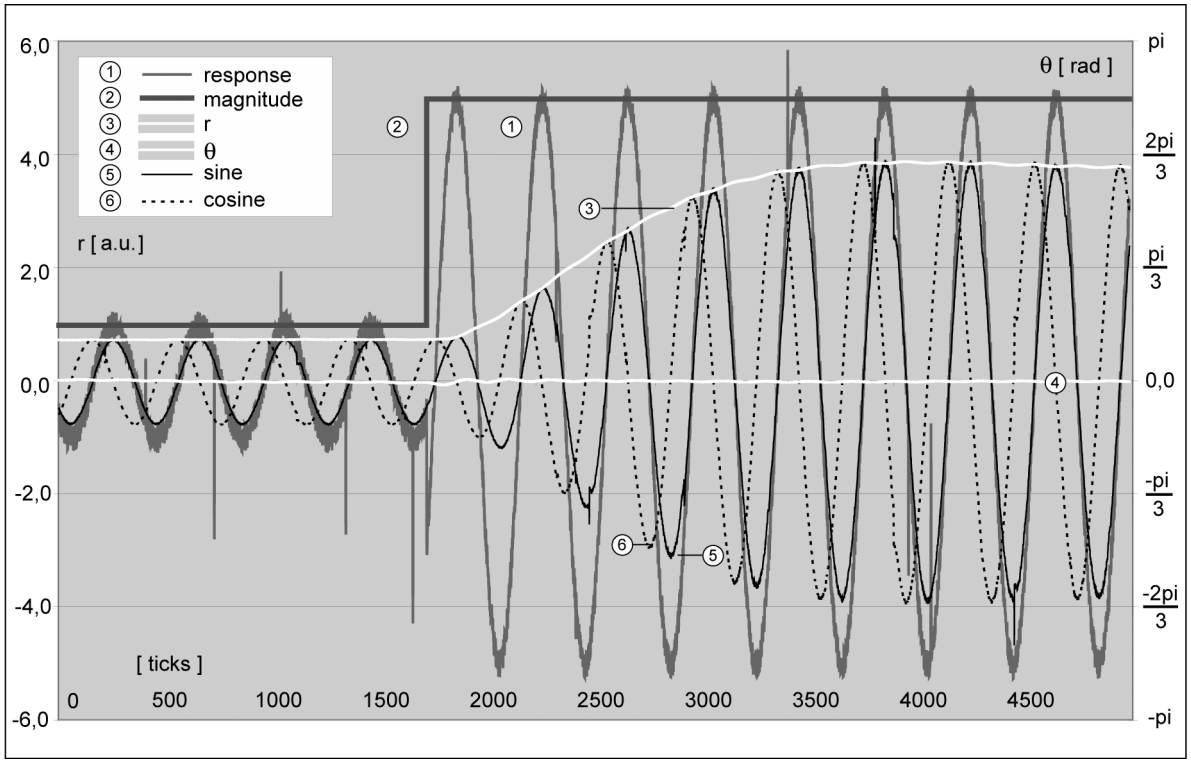

Figure 4.1.8 : *Digital lock–in amplifier PSD output swing following a system response step up.*

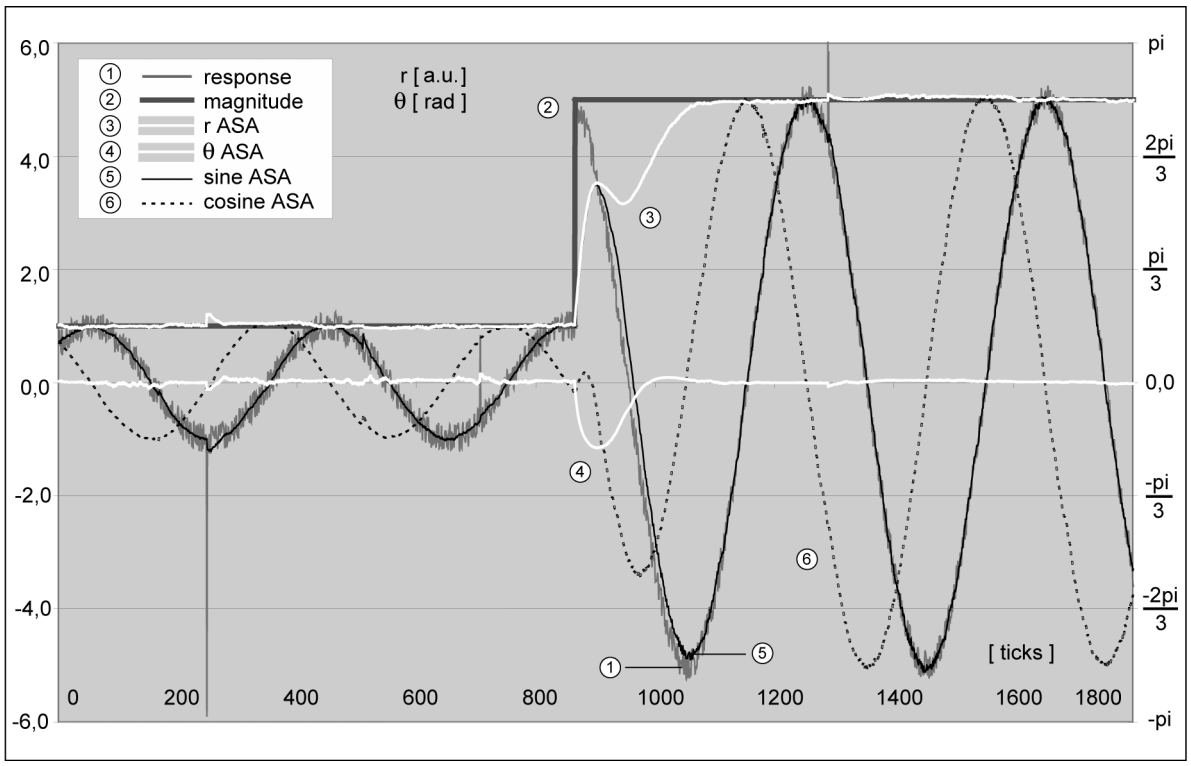

Figure 4.1.9 : *Single line ASA filter adaptation on equal magnitude step.*

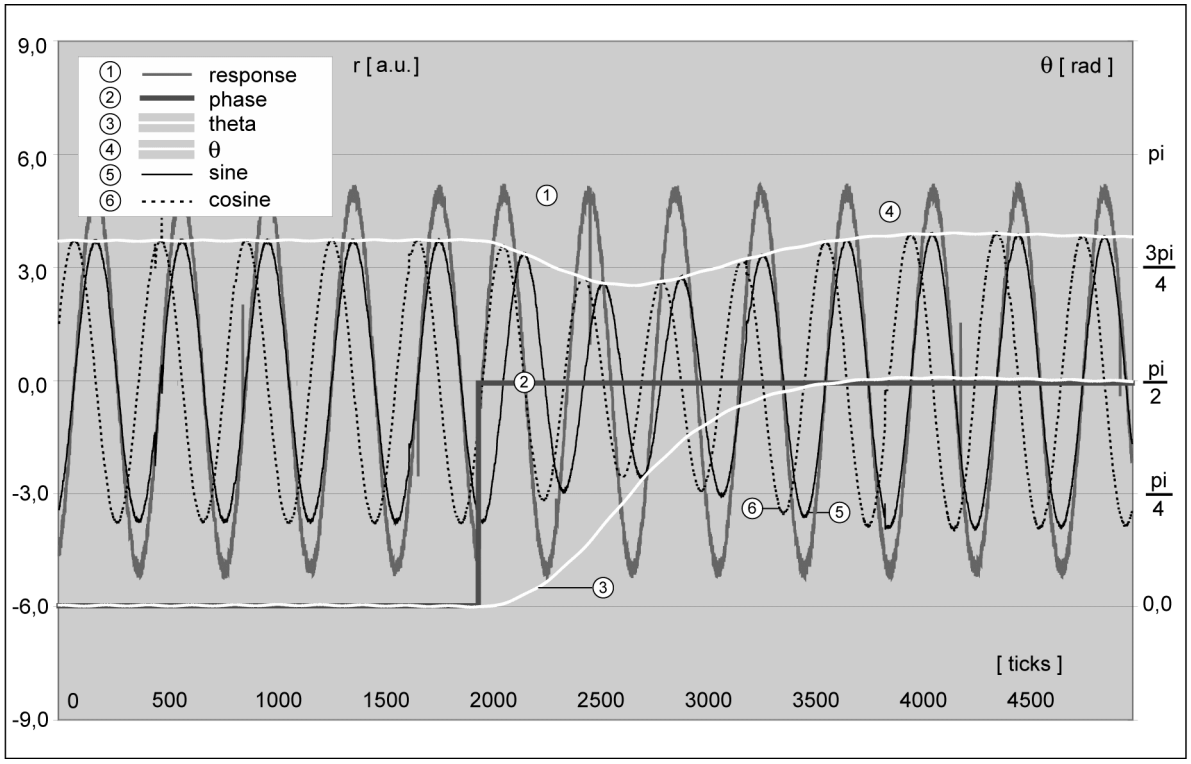

Figure 4.1.10 : *Digital lock–in amplifier phase output on a step from 0 to 90 degrees.*

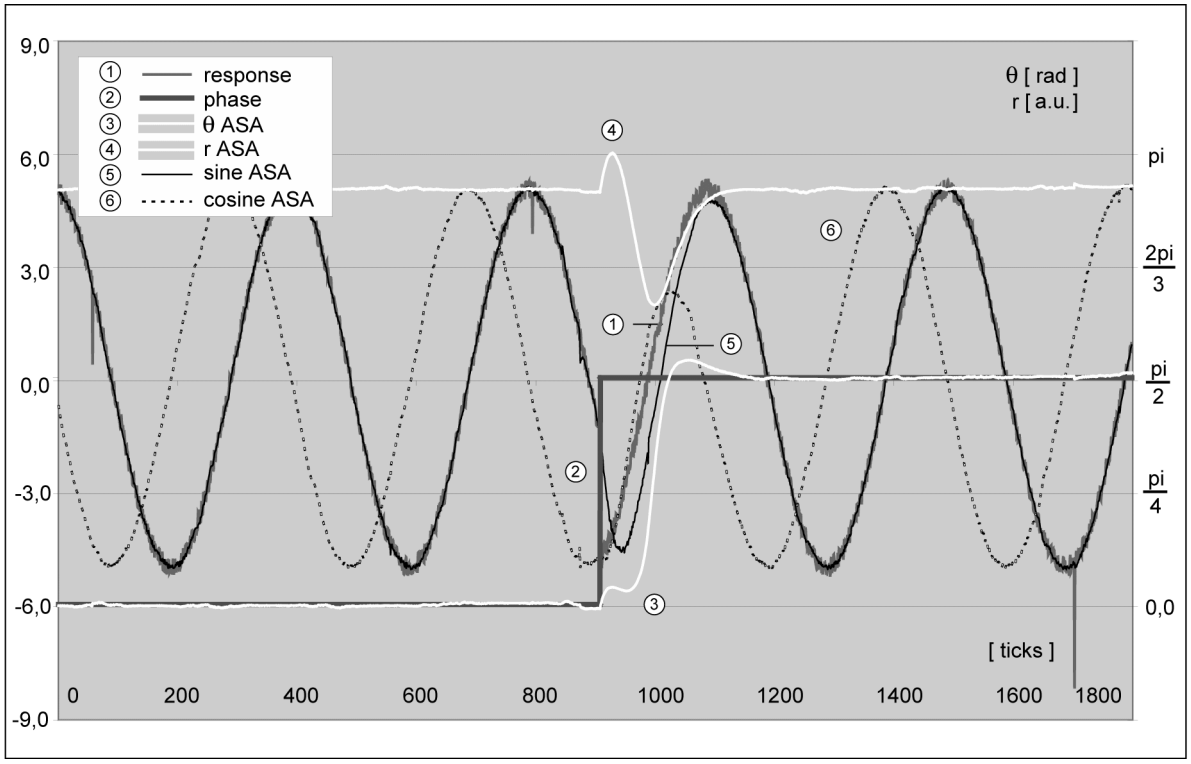

Figure 4.1.11 : *Single line ASA filter adaptation on identical phase step.*

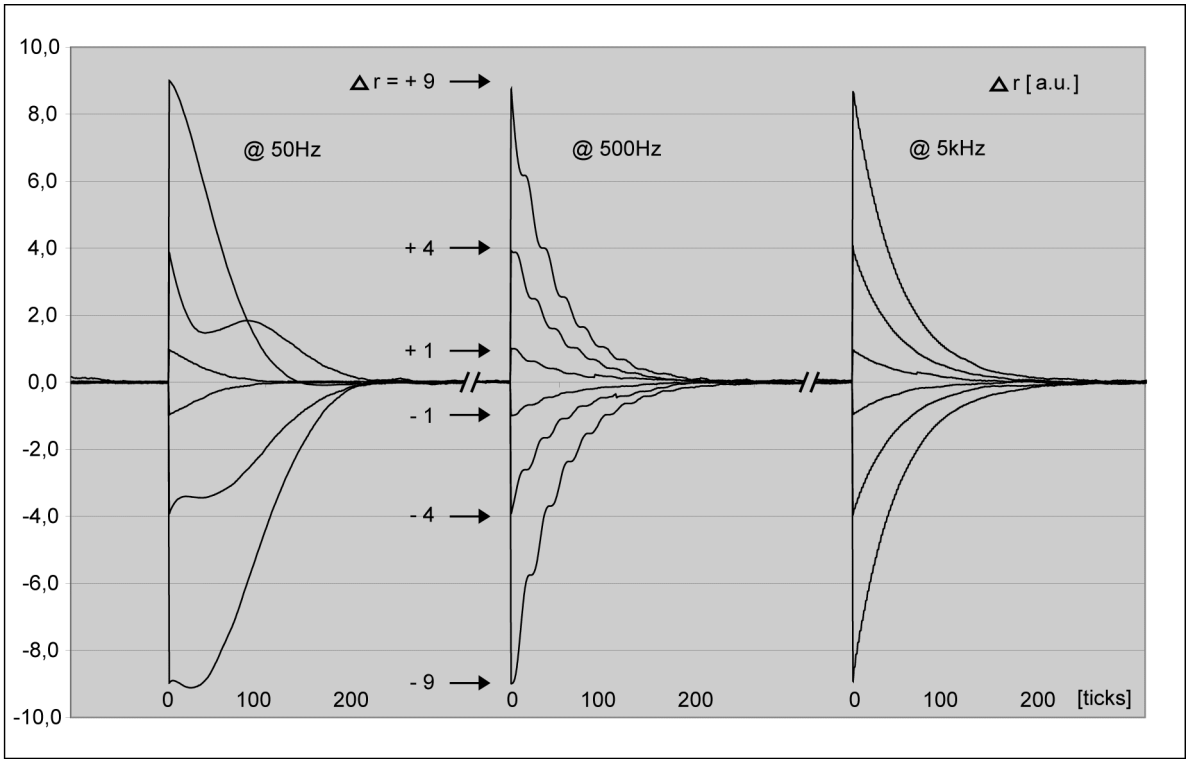

Figure 4.1.12 : *Exponential decay of the ASA magnitude identification error. The error transient is recorded for bidirectional step heights from 1 to 9 arbitrary units. The experiment runs at the specified modulation frequencies.*

To conclude the paragraph we clarify how the adaptive filter reacts on different step conditions. Height and direction are varied. As phase and magnitude steps are executed at higher modulation frequencies fig. 4.1.12 and fig. 4.1.13 reveal that the decorrelation time is a filter constant. It follows from the statistical assumptions on the system and measurement noise in the state space model of the Kalman filter [6] and acts as the counterpart of the integration time in the lock–in amplifier analysis technique. In accordance to fig. 4.1.9 the decorrelation time is approved at value 200 ± 20 ticks. Similar to the lock–in principle the course of the identification error gets ripple free as the ratio of decorrelation time and modulation period increases. Related to the given sampling frequency of 20 kHz we have:

$$@\ 50\ \text{Hz}: \quad \tau_{decorr.} / \tau_{mod.} = 0.5 \qquad @\ 5000\ \text{Hz}: \quad \tau_{decorr.} / \tau_{mod.} = 50.0 \tag{4.9}$$

It is clear that the excellent decorrelation properties of the stochastic statement provides a new spectral analysis tool that will unfold its full performance in particular when used in a time critical online application. But due to the fact that the dynamics can be tailored to the experimental demand it is also first choice in a noisy and distorted measurement environment. It is left to point out, that the concept can handle the synchronization as well the identification task, thus it reduces the tool box to one Swiss knife.

6 remember subsection 3.1.3

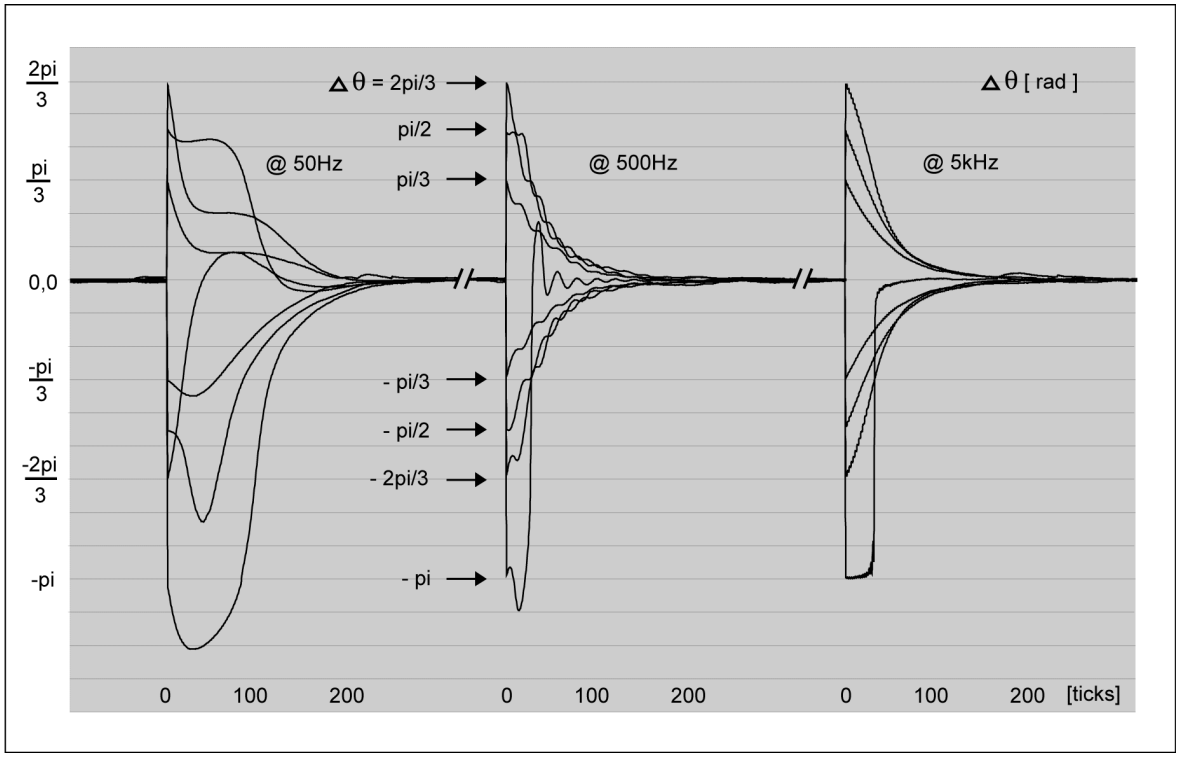

Figure 4.1.13 : *Decorrelation of the ASA phase identification error. The error transient is recorded for bidirectional step heights from pi/3 to pi in radians. As with the magnitudes the typical decorrelation time is 200 ± 20 ticks.*

4.1.3 Resonance Curve Recordings

Next the ASA filter will be employed to measure the mechanical transfer function of a commercial piezo scanner. The setup has already been introduced at the beginning of the subchapter and is depicted in fig. 4.1.1. The test object is a 3–axis nano actuator from *piezosystem jena* [7] that is applied in nanooptics and metrology to support ultra precise object motion on a nanometer scale. The stage is also widely used in scanning probe microscopy instrumentation. The embedded piezo ceramics (lead zirconate titanate, LZT) are orthogonally arranged in a mechanical housing. As an external electric field is applied, the inverse piezoelectric effect makes the ions shift in the crystal lattice. They move in new positions where the shear compensates for the electrical forces and the crystal relaxes into equilibrium state [PAE96]. Slip and friction free translation of the nano positioner's top mounting plate (bright aluminum, fig. 4.1.14 a, circled zone) features solid state flexure hinges. Tension caused by the piezo elongation makes the hinges bend [VOR01]. The plate is screwed and follows the motion linearly. It is set into normal vibrations through a periodic electrical stimulus which is synthesized by a Hewlett Packard 3325A waveform generator. The instrument supports sine wave synthesis with a minimal peak amplitude of 1 mV in the frequency range of interest from 1 Hz to 2.5 kHz. As the piezoelectrical translation ratio of the nano positioner is 1 µm/V a static control voltage of 1 mV yields a

7 TRITOR 100

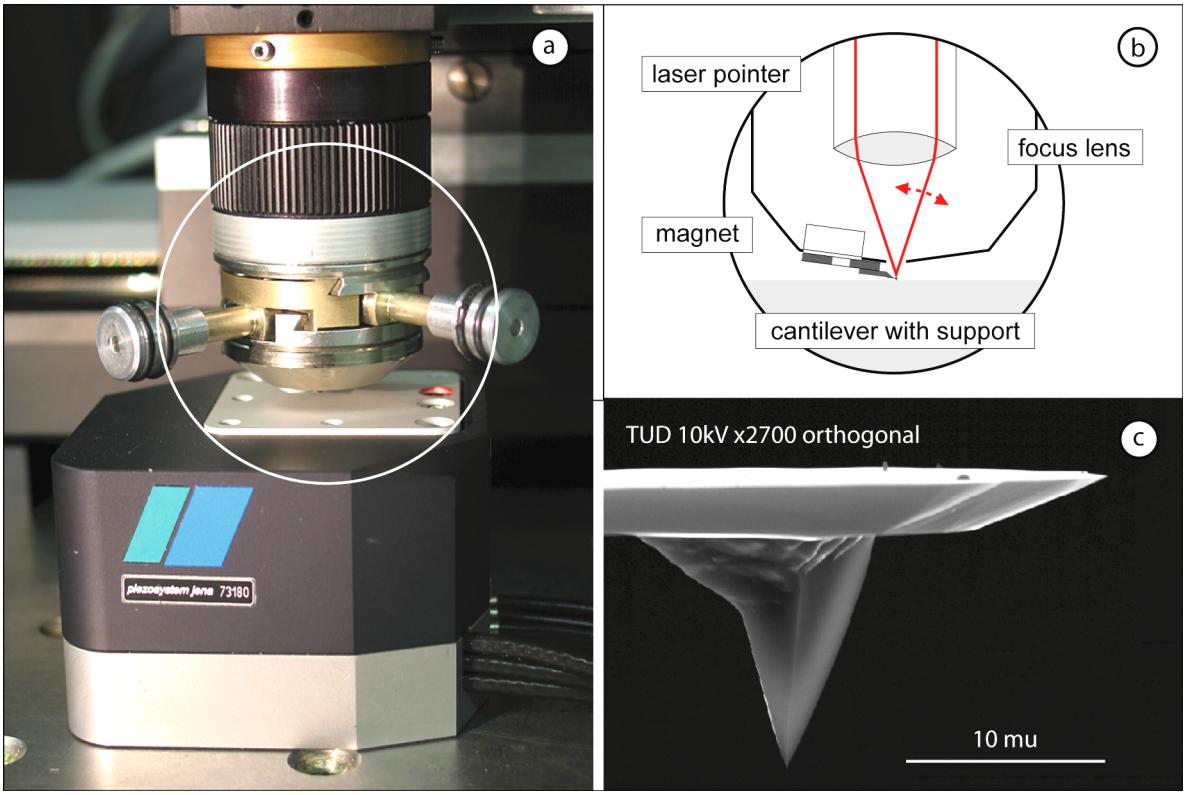

Figure 4.1.14 : *Resonance recording metrological hardware and test object.*

nominal translation of 10 nm. So according to its specifications the waveform generator is apt to drive ultra low surface oscillates. The modes on the mounting plate are sensed by the nanocartographer as described in chapter 2. The quadrant detector of the AFM sensor supplies an output voltage proportional to the oscillation amplitude which is connected to the analog interface of the signal processing hardware. For reference the experiment is repeated on the output of the built in capacitive position sensor. The response analysis algorithms run on the Analog Devices ADSP21160 evaluation board imaged in fig. 4.1.15. On board codecs ADC1 and ADC2 sample the system stimulus respectively the response at 20 kHz. The DSP is clocked at 80 MHz, thus 4000 core computations may be executed per loop cycle. This is in accordance to the computational demand which is far less [8]. The experimental schedule starts with an approach of the AFM sensor to the surface of the mounting plate, whereas the z–coordinate of the microscope objective is automatically controlled and gradually changed by the nanocartographer as shown in fig. 4.1.14 a. Meanwhile the stimulus is switched off. As the cantilever touches the mounting plate the actuator position control hardware reacts and lowers the plate by piezo motion to keep the atomic forces constant. Fig. 4.1.14 c depicts a scanning electron microscope image of the nanooptical device taken at the institute. As the plate has moved downwards 50 micron, which is half the maximum translation range of the piezo actuator, linear translation of the microscope objective stops. Next the position control of the actuator is switched to a tailored constant height mode. We activate the stimulus now and the output of the

8 The number of assembly instructions to compute the ASA filter output on the ADSP21160 microcomputer is 76.

AFM sensor starts to oscillate as illustrated in fig. 4.1.14 b. Tailored height means, that the z–coordinate of the mounting plate is adjusted slowly, such that the sensor signal is kept mean free during the resonance experiment. This eliminates mechanical creep and temperature drift in the nano cartographer instrument.

The data of the resonance scan is depicted in the graphs of figures 4.1.16 and 4.1.17 where magnitudes and phasing are plotted as measured by the atomic force microscope and the capacitive position sensor. The spectrum is acquired between 1 Hz and 2.5 kHz in a linear frequency ramp over a wobble time of 100 s. The lines are stored in a buffer on the external memory of the signal processing hardware. Each 40 ms a new capture of the ASA filter kernel is taken. Thus we get a comb of 2500 lines with a frequency spacing of 1 Hz. The stimulus is set to 1 mVp. After completion the acquired data is transferred to a computer via USB interface for post processing and documentation.

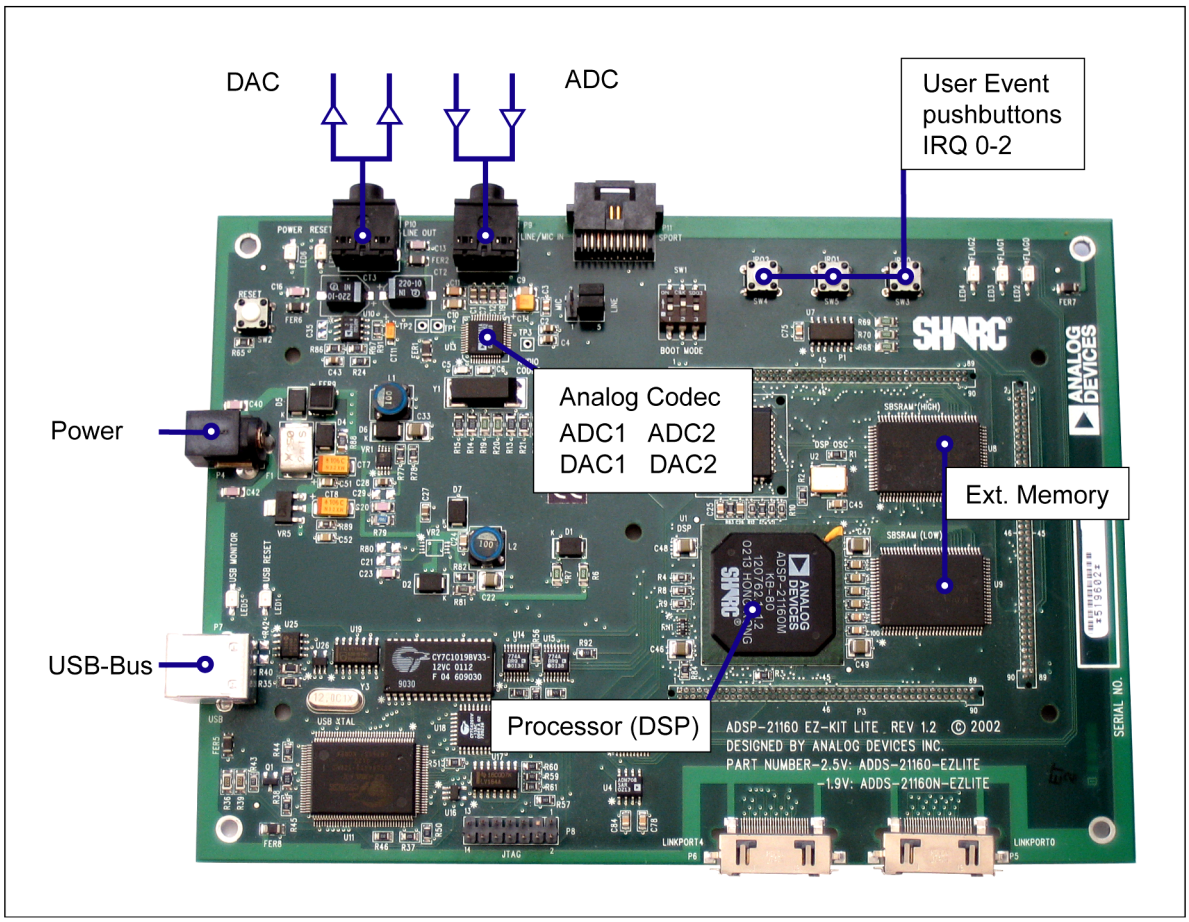

Figure 4.1.15 *: Resonance recording digital signal processing hardware. Preliminary performance analysis of the DSP algorithms is feasible by synthesizing the stimulus with the digital to analog converters DAC1 and DAC2. The signals are looped back via audio cable to the analog to digital converters ADC1 and ADC2. Digital noise and spurs can be added in the signal path to check robustness.*

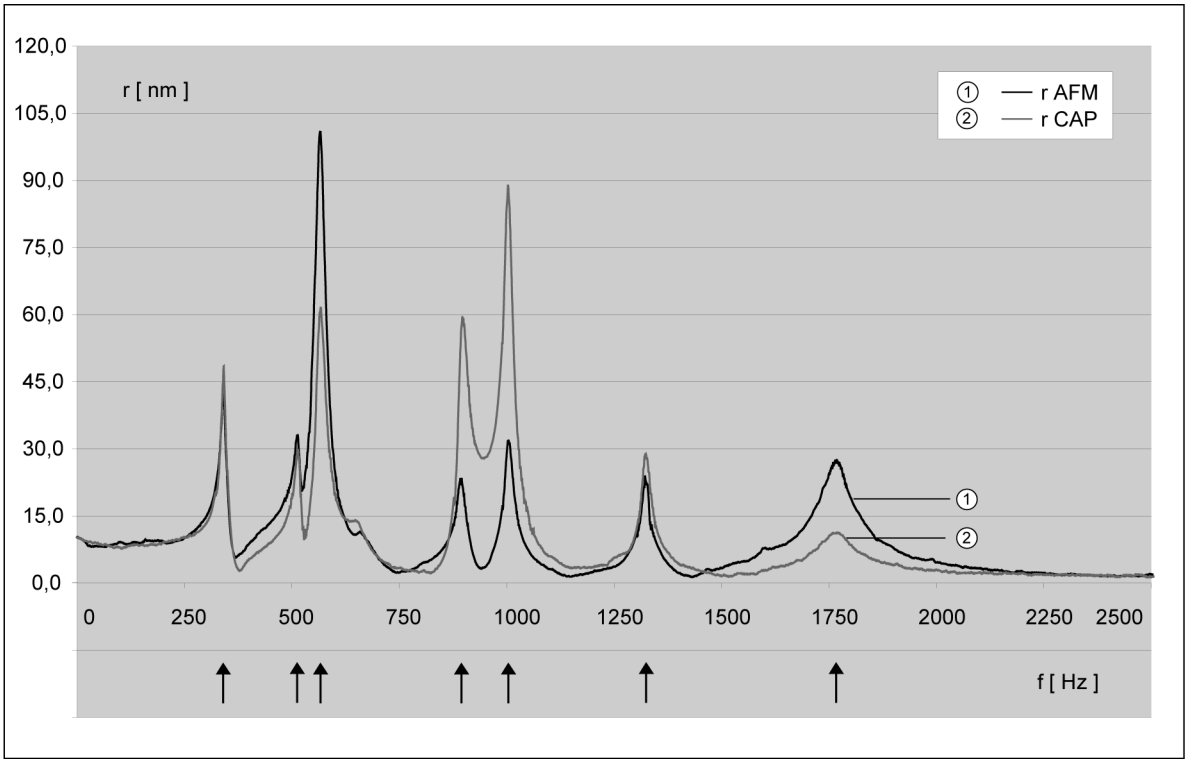

Figure 4.1.16a *: TRITOR 100 piezo actuator resonance curves part I. Oscillation magnitudes in z–direction are characterized by adaptive spectrum analysis. The plot data originates from the nanocartographer (AFM) respectively the actuator's built in capacitive position sensor (CAP). The AFM measures the resonance at x–coordinate 10.0 mm ± 200 nm and y–coordinate 0.0 mm ± 200 nm right of the plate center.*

Both instrumentations detect the spectral peaks at equal frequencies. The maxima are indicated by upwards directed arrows. They act as a post mark in the follow up diagrams. We count 7 spectral peaks in the frequency range up to 2.5 kHz which means the transfer function has at least 7 poles in the complex plane near of the unity circle [GRUE01]. The magnitudes differ between the sensing technologies which is explained by two facts. First the AFM resolves the response *lateral microscopic* whereas the CAP sensor integrates the oscillation *lateral macroscopic* due to the geometric dimensions of the sensor devices (see fig. 4.1.14 a and c). Second the Chladni patterns are spreading several centimeters on the plate surface and the sensors quantify the resonance phenomena at different cartographic coordinates. This statement is supported by a whole series of magnitude profiles recorded at master coordinates. A coordinate change of the nanocartographer requires to lift up the microscope objective 100 micron before horizontal translation. After that the approach schedule has to be repeated. The procedure takes about 30 s. The resonance curves shown in fig. 4.1.16 have been recorded within 7 minutes time. The frequency range was further extended to 20 kHz for survey. A resonance peak of magnitude 13 ± 2 nm was observed with the AFM sensor at 15.1 kHz. But this is far beyond the specified bandwidth of the CAP sensor electronics, which is 2.5 kHz, so the data is not considered here.

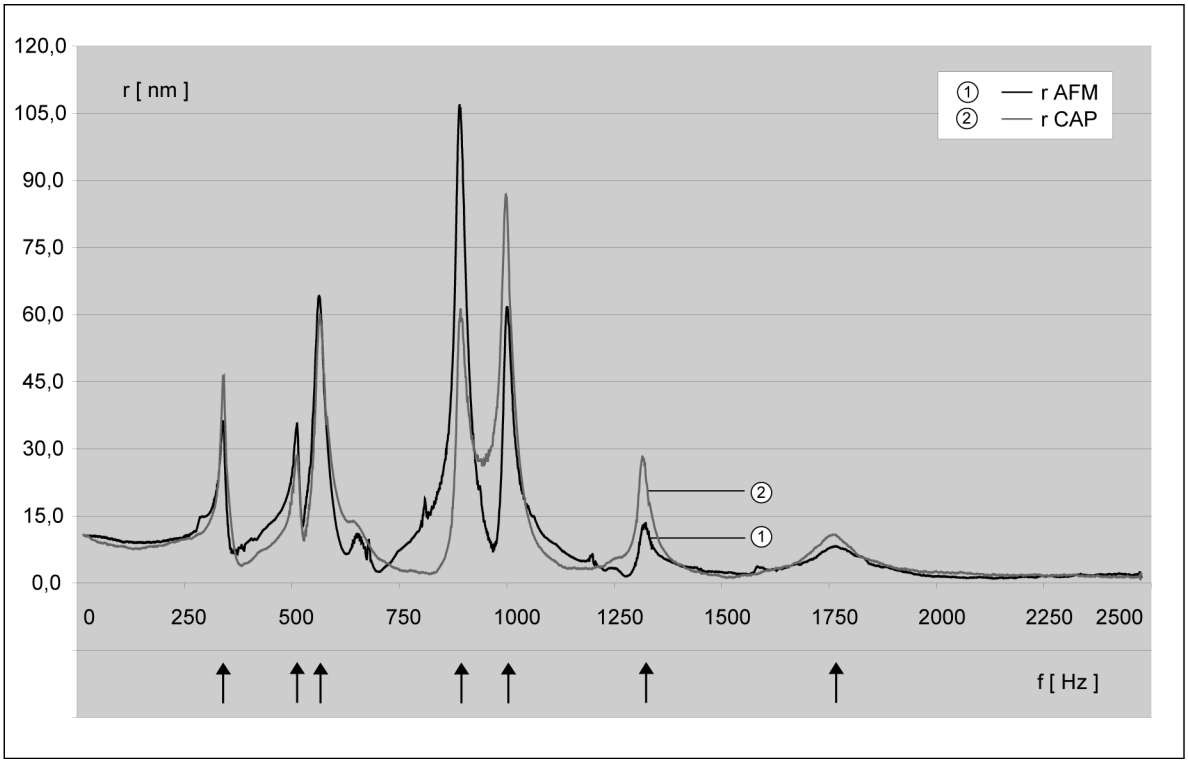

Figure 4.1.16b : *TRITOR 100 piezo actuator resonance curves part II. The AFM resolves the modes at x–coordinate 0.0 mm ± 200 nm and y–coordinate 0.0 mm ± 200 nm in the plate center. Changes of the CAP data points to the previous plot can be neglected.*

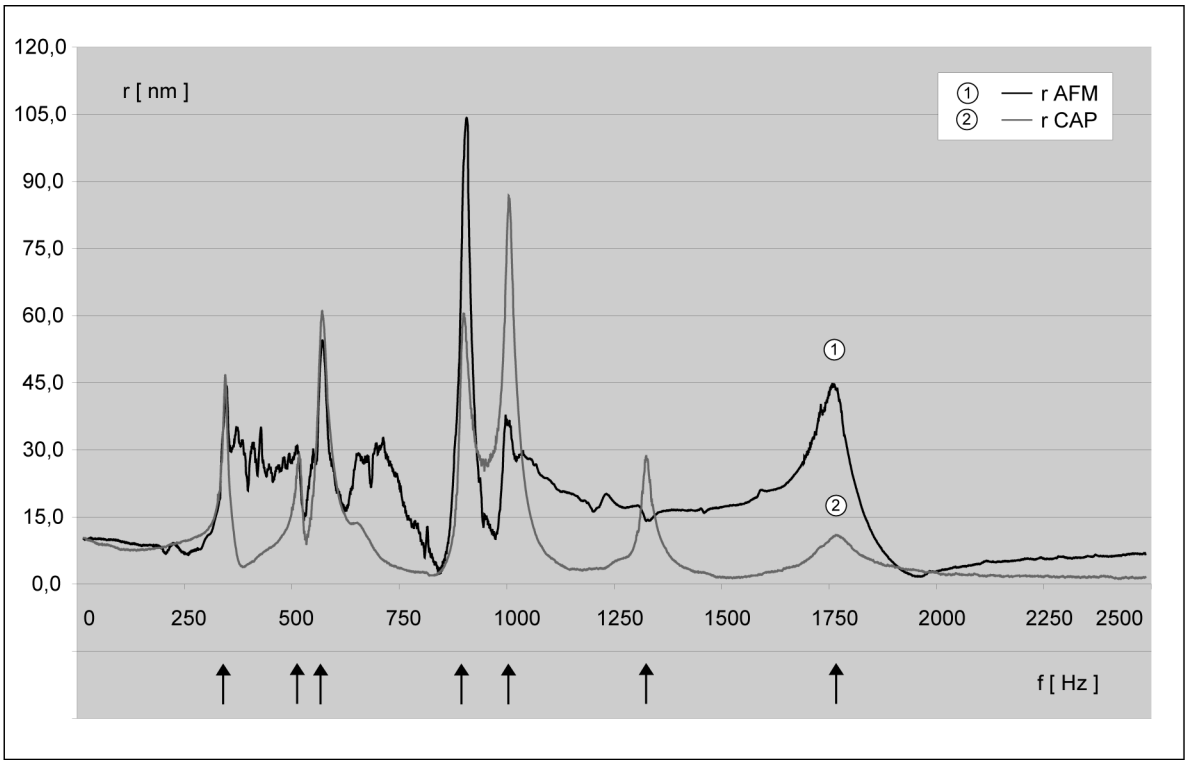

Figure 4.1.16c : *TRITOR 100 piezo actuator resonance curves part III. The AFM senses the magnitudes at x–coordinate –10.0 mm ± 200 nm and y–coordinate 0.0 mm ± 200 nm left of the plate center.*

Phasing is even more closely connected for both sensors. The curves in fig. 4.1.17 reveal typical phase transitions of $-\pi$ at the dominant frequencies known from the damped harmonic oscillator model. The transitions of $+\pi$ pointed out by the downwards directed arrows do not show an equivalent peak in the above magnitude plots. They indicate a confined nonlinearity of the mechanics, precisely spoken an energy dissipation of the stimulus into higher modes, which is also clearly visible on a scope connected to the setup for monitoring. AFM and CAP data differ in a phase key $\Delta\theta$ that is due to a considerable signal delay Δt in the capacitive sensor electronics meeting the formula

$$\Delta\theta = 2\pi f \cdot \Delta t \tag{4.10}$$

The delay is extracted from the data as $\Delta t = 350 \pm 18\,\mu s$ which is a drawback as compared to the undelayed AFM sensor signal.

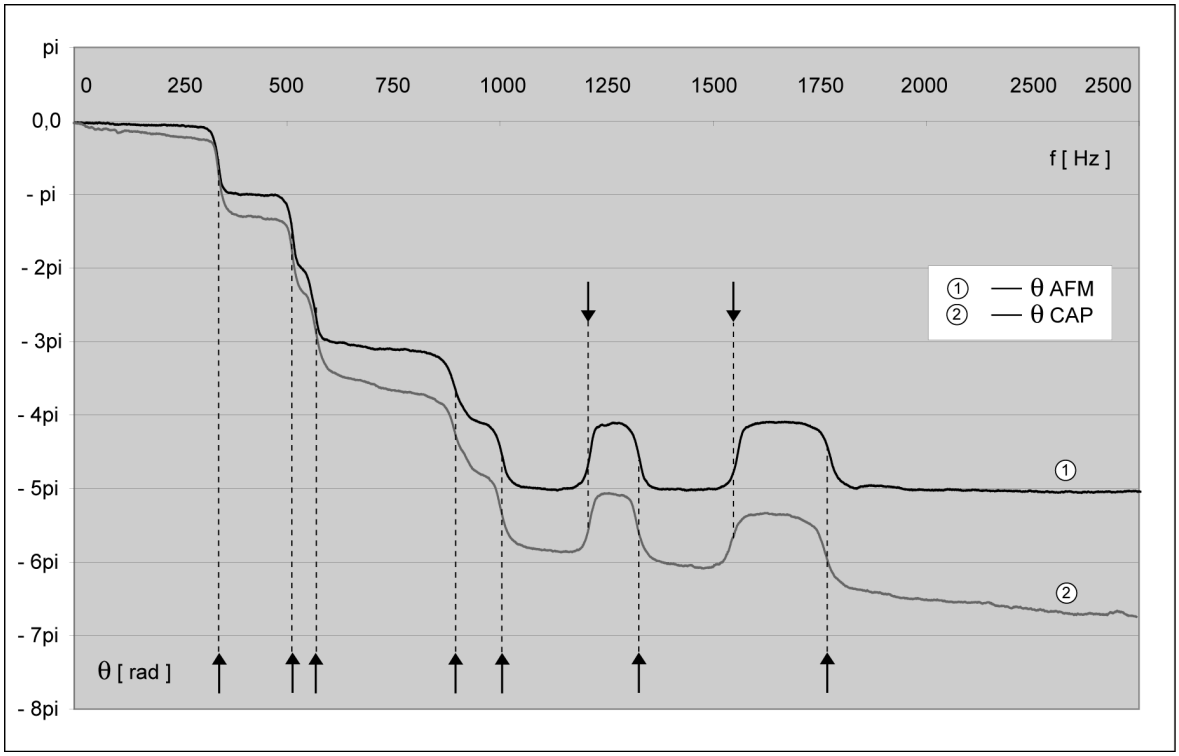

Figure 4.1.17 : TRITOR 100 piezo actuator resonance phasing. The AFM measures the phasing at x–coordinate 10.0 mm ± 200 nm and y–coordinate 0.0 mm ± 200 nm right to the center of the plate.

Now that we are well grounded in a full dynamic characterization of the nanooptical model system, the multi line ASA filter operation can be studied under various broadband system stimuli.

4.2 Broadband Spectral Adaptation

It has been pointed out in the theoretical discussion of the ASA filter method that the true innovation of this work is the tremendous reduction of the numerical effort as compared to prior known high performance adaptive filter techniques. However up to now we merely know that it is *technically feasible* to run the filter at high analytical orders. The decisive question remains to be answered : Do we really benefit from that when using the tool to explore the physics of higher dimensional systems ? The issue cannot be solved in general here. The nanooptical model system has been selected with great care. It is nontrivial to characterize and the experiments in the previous section reveal indeed that it has the high degree of complexity value 6.3 [1]. But the physics are known and well understood. This is mandatory since the mission is to quantify the qualities of the new approach in a rigorous manner. So starting from scratch the answer has to be broken down, whether the ASA filter as compared to the spectral analysis standard is *methodically favorable*. We treat this in form of DSP microcomputer simulations. To explain: a DSP simulation runs the algorithm to be qualified on the same target platform as employed later in real life experiments. However sensor data streams are replaced by a meaningful signal model which is also computed on the embedded target. Model rates can be much slower than sensor ones thus runtime is not critical. The simulation may be seen as a slow motion of the experiment. In the sense of chapter 3 the emulation however is executed *online*. One major advantage of a DSP simulation is based on hardware and software integrity of the spectral analysis application to be verified. In case of a computer simulation everything is done on a host processor unit *offline* so latter option misses. In order to synthesize the actuator response by means of the prior measured mechanical transfer function we define an arbitrary spectral stimulus. A complex unity oscillator base is created at the stimulating frequencies. The response model is based on convolution. Each NCO member is complex weighted by the assigned spectral line. Magnitudes and phasing at points of interest are determined by means of a spline interpolation [2]. The emulated response continuously sets from the sum of real parts. As the stimulus and the analysis NCO ensembles are equal we note that *coherent*, otherwise *incoherent,* system irradiation.

We start with the following simulation parameters:

DSP clock	80 *MHz*	stimulus magnitudes	1 *mV* / NCO
sampling rate	20 *kHz*	stimulus phasing	0 ... 2π (random)
virtual loop time	50 *μs*	frequency range	1 ... 2048 *Hz*
stimulus NCO	2048	response noise level	50 *nm* rms
analysis NCO	2048 (coherent)	response spike level	1 *μm* rms

1 For system size the geometry of the top mounting plate is taken. The minimal structure size is declared from the smallest spectral peak magnitude. Thus according to fig. 4.1.16 the degree of complexity as introduced in chapter 2 equals :

$\log(2 \cdot 10^{-2} / 10 \cdot 10^{-9}) = 6.3$

2 Annotation : the resonance curve of the piezo actuator has been recorded at 2500 frequencies from 1 to 2.5 kHz with a spacing of 1 Hz. See figures 4.1.16 and 4.1.17.

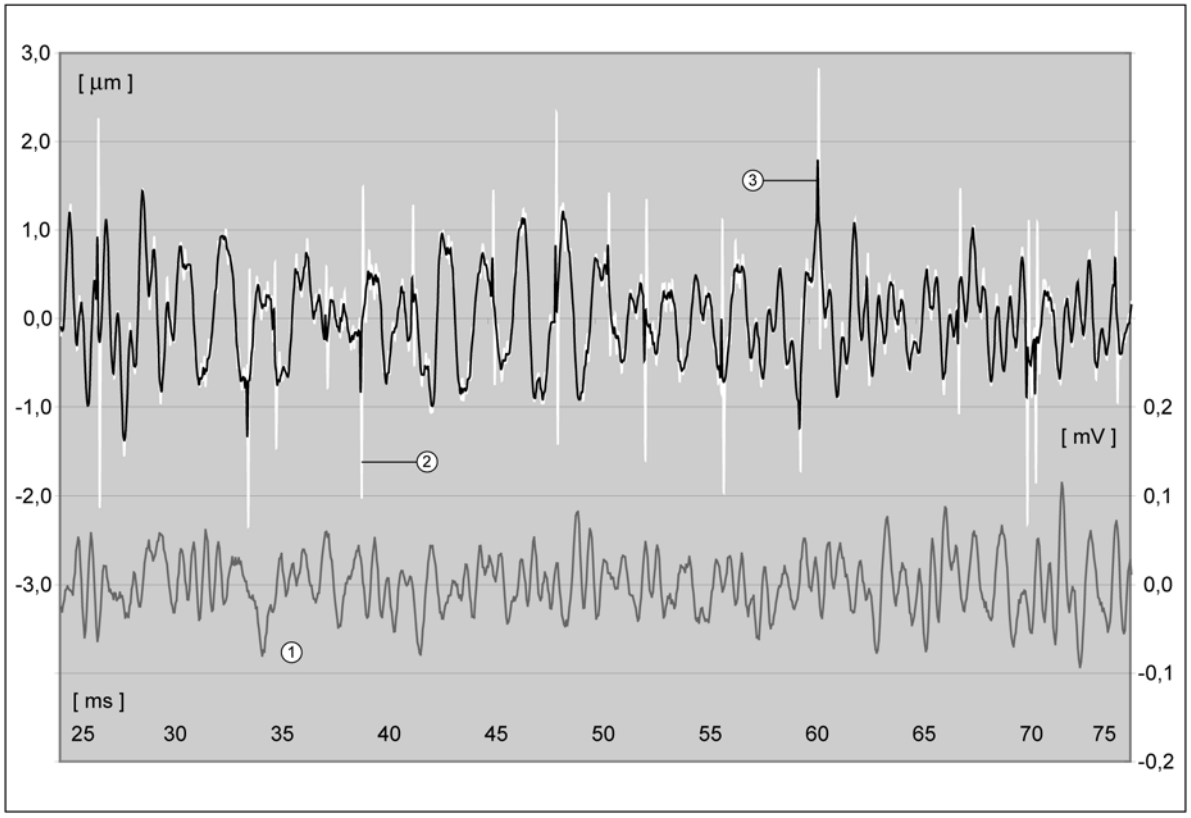

Figure 4.2.1 : *Adaptive spectrum analysis input and output signal courses. The system stimulus* x *irradiates the complex transfer model of the nanooptical system. The model response* r *and the output* y *of the ASA filter are in very good agreement.*

The ASA filter needs to be initialized. The vector of gain magnitudes $|g\rangle$ and the phase encoding profile $|\theta\rangle$ both have been measured according to the instructions summarized in tab. 3.2.2 . The filter kernel $|w\rangle$ is cleared before the simulation starts. First we study in time domain, how the ASA filter output approximates the model response. Time courses of the relevant signals are depicted in fig. 4.2.1.

As expected from the experiments reported on single line adaptation, the multiline ASA filter also decorrelates very fast. Above data set has been captured 25 ms after simulation startup and covers 50 ms on the time line. The adaptation is visibly insensitive to uncorrelated distortions in the signal path like white noise and spurs. Since the phasing of the stimulus has been randomized at startup the variance of the driving amplitude is homogeneous. This is intended for the experiment and advantageous with respect to the sensor linearity. Above snapshot is judged to be representative for stimulus, system response and adaptive filter output. Courses do not alter the distinguishing characteristics on the future time line. If we compare the spectral match of the filter kernel and the model spectrum at the same instance in time (see fig. 4.2.2 and fig. 4.2.3 top graph) we find in conflict a very poor concurrence in magnitudes and almost none in phasing. This asks for an explanation.

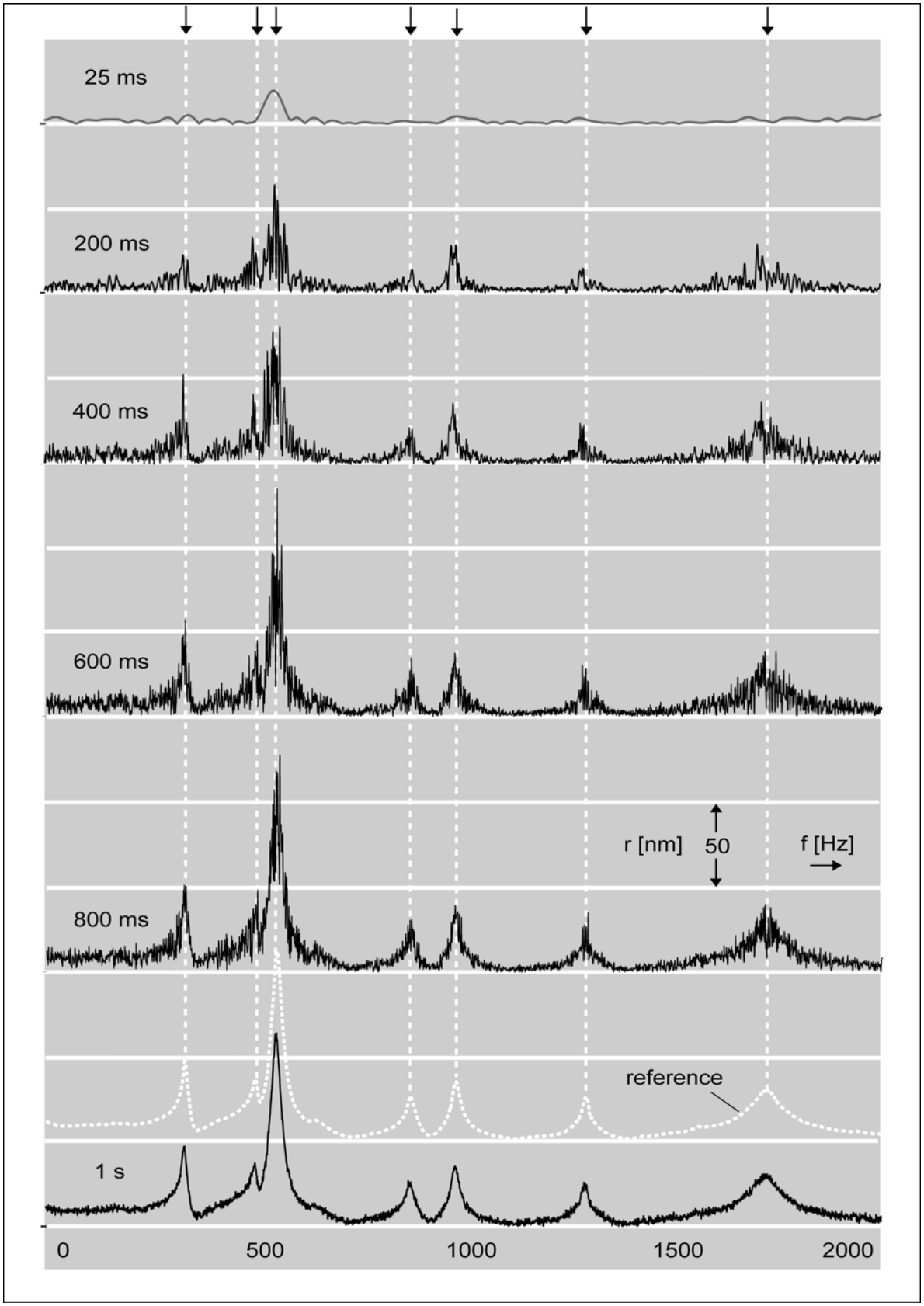

Figure 4.2.2 : *Evolution of the spectral magnitudes at coherent stimulus. The transfer model magnitudes are added to the plots for reference in dashed white line. The profile already indicates in the adaptation process after 200 ms and is fully developed after 1 s.*

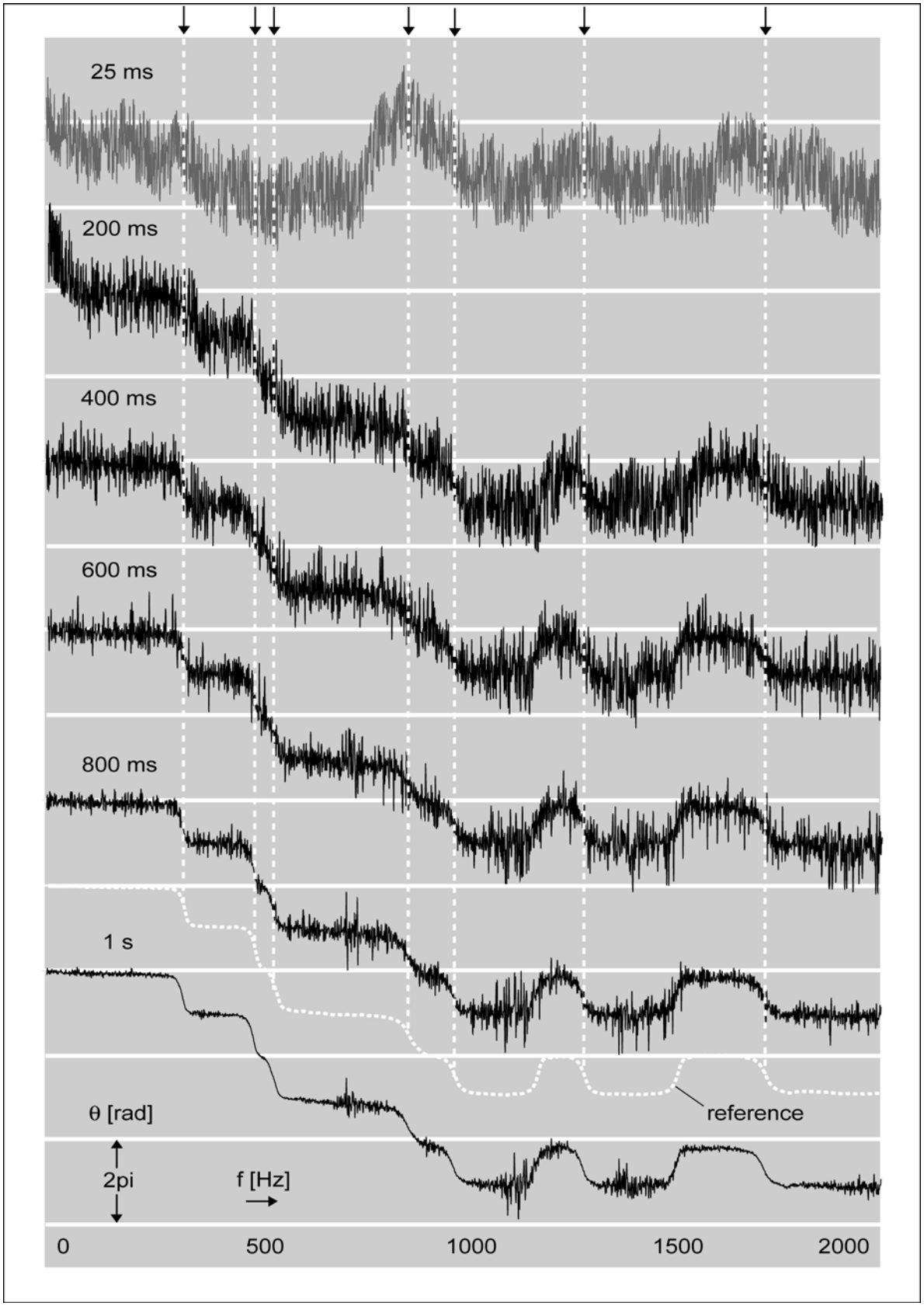

Figure 4.2.3 : *Evolution of the spectral phasing at coherent stimulus. The qualitative course is clearly visible after 200 ms. Phase noise almost completely fades out after 1 s observation time. The transfer model phasing is shown in dashed white line.*

We notice that adaptive filter NCOs twiddling at other frequencies than the spectral peak ones share a partial coherence with model NCOs that do rotate on the dominant frequencies. The coherence makes the corresponding lines in the filter kernel rise. As a matter of fact the spectral signatures in the model response are synthesized by line subgroups at the cost of time varying phase. This mechanism is the reason why the response signal is approximated correctly though the synthesizing magnitudes are far smaller than expected. It is also root of the phasing mismatch. As time ticks both kernel magnitudes (fig. 4.2.2) and phasing (fig. 4.2.3) settle on an excellent adaptation of the model spectrum after 1s. This equals the period of the base oscillator on the frequency comb.

Next the simulation is repeated with an incoherent stimulus. The previous parameters are kept except from a modification of the stimulus oscillator ensemble which is extended to 3500 members. The new spacing on the frequency comb is 0.585 Hz. Fig. 4.2.4 unfolds the evolution of the ASA magnitudes estimation error. Similar to the coherent scenario the filter operation enters a steady state after 1 s observation time. Stationarity is detected from the estimation error turning mean free. The magnitudes profile shows a strongly developed ripple that once again is rooted in partial coherence effects [3]. The analysis oscillators are in a competition. Some show a higher coherence to the model and others do not. Prior win while latter loose being suppressed by the tuning mechanism of the ASA filter.

However we can reconstruct the model spectrum based on the acquired state of the adaptive filter kernel. Think of a single spectral line. The one adaptation will be driven by all stimulating NCOs in a confined frequency neighborhood. Assume further the influence to decay exponentially with the frequency distance in accordance to a partial coherence theorem. Then the magnitude obeys the formula :

$$r_K(f_K) = \frac{\sum_{j=0}^{N-1} \tau^{\frac{|f_K - f_S|}{f_K}} \cdot r_M(f_S)}{\sum_{j=0}^{N-1} \tau^{\frac{|f_K - f_S|}{f_K}}} \tag{4.11}$$

whereas

r_K	:	ASA filter kernel spectral line magnitude
f_K	:	spectral line frequency
r_M	:	model response magnitude
f_S	:	stimulus frequency
τ	:	exponential coherence weight

An approximation of the model response magnitude can be found through a bidirectional exponential smoothing of the measured ASA filter kernel in frequency domain [SMI99].

3 annotation : phasing is invalid thus not treated

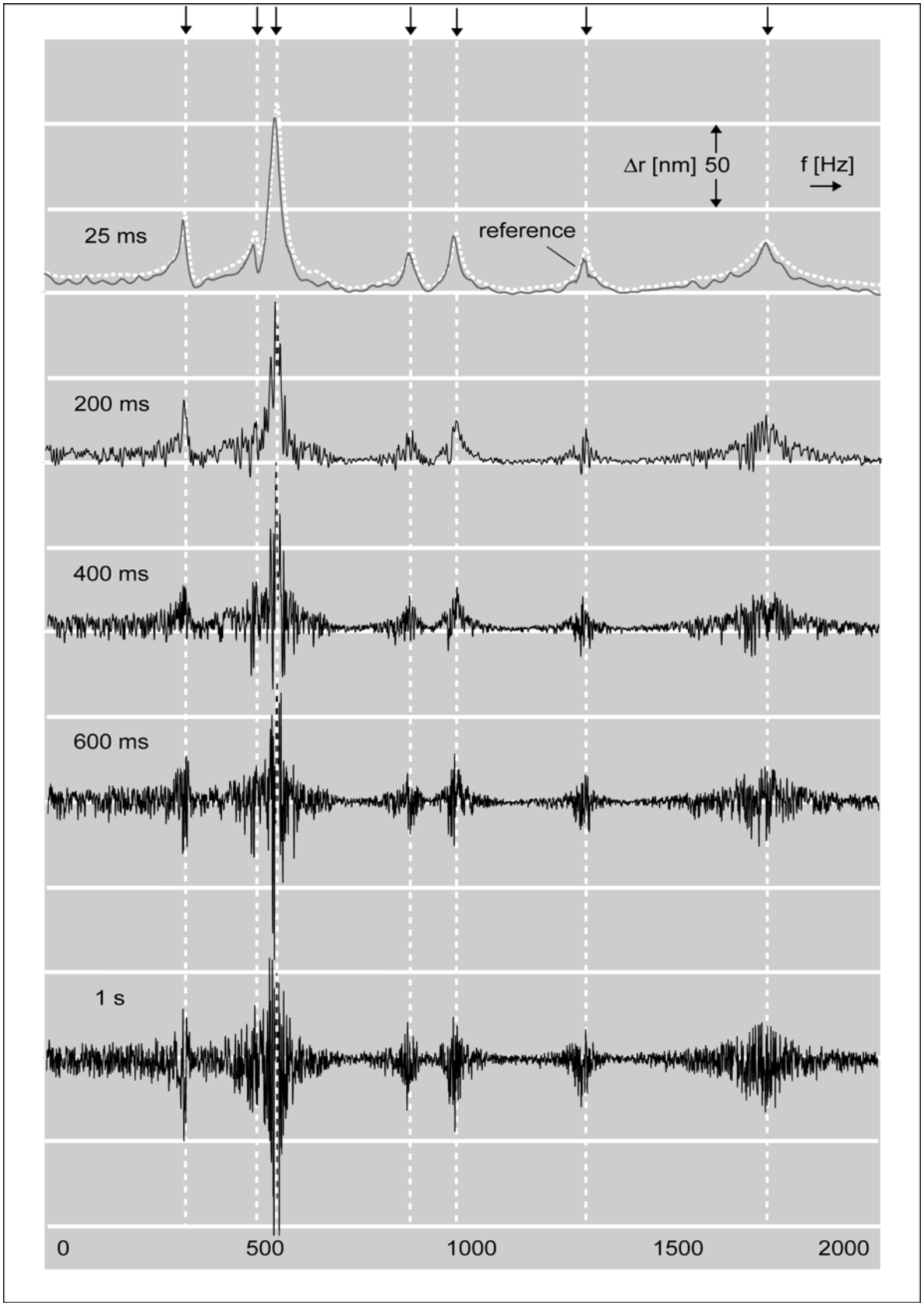

Figure 4.2.4 : *Exponential decay of the magnitudes estimation error at incoherent stimulus. After 1 s the spectral error is mean free. But it keeps a ripple in the adapted state, that is due to partial coherence of the stimulation and identification oscillator ensembles.*

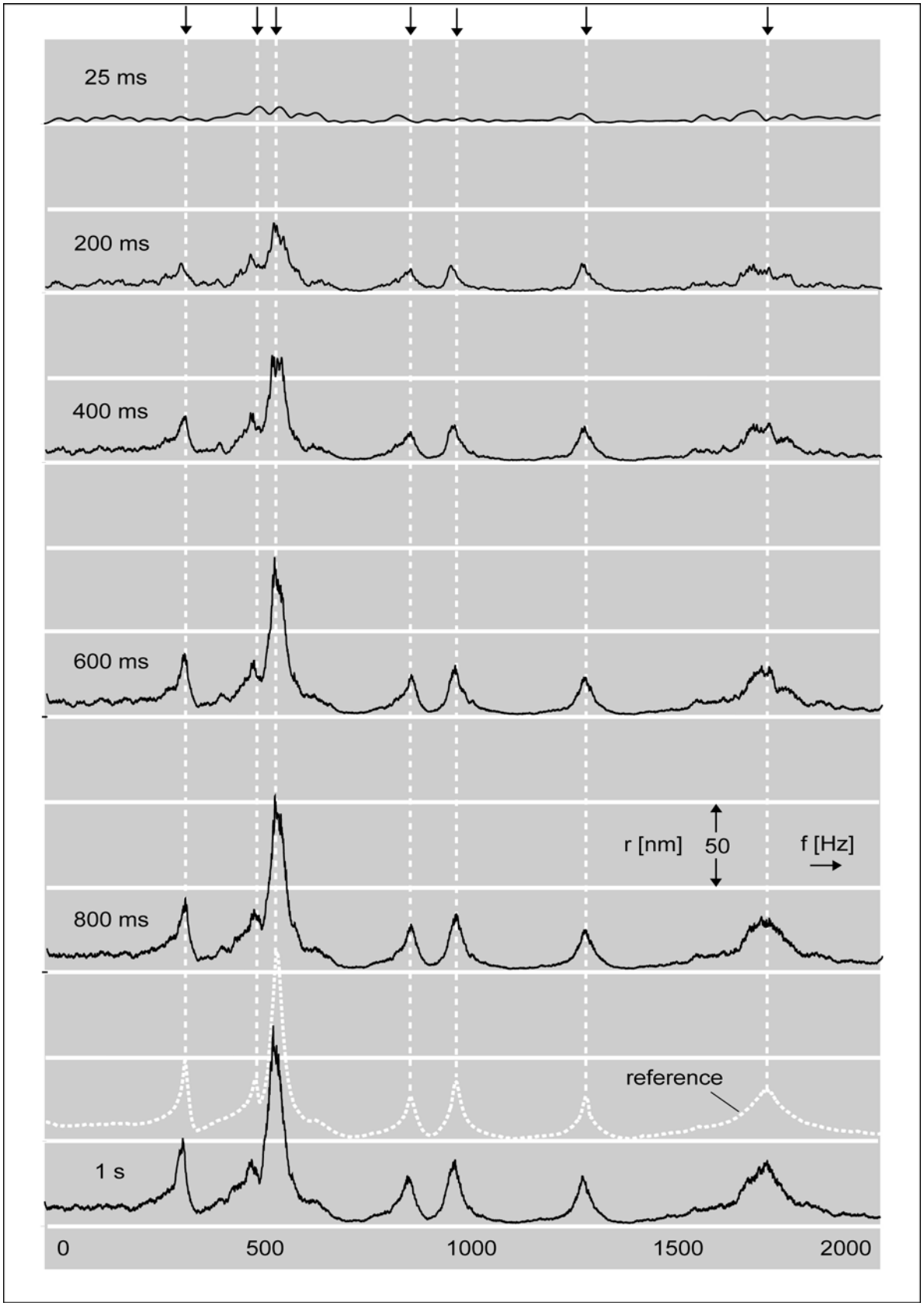

Figure 4.2.5 : *Reconstruction of the piezo actuator model spectrum from the measured data in case of an incoherent system stimulus. Latter incorporates a partial coherence assumption for the harmonic processes in the ASA filter and the nanooptical system.*

The reconstruction r_M^* follows in iteration. Frequencies higher than the spectral line in focus are said to form the *spectral highband*, otherwise they are noted as the *spectral lowband* . The estimate of the model at the reconstruction frequency constitutes from a highband (HB) and a lowband (LB) term of equal weight as shown :

$$r_M^{HB}(i) = \tau \cdot r_M^{HB}(i+1) + (1-\tau) \cdot r_K(i)$$

$$r_M^{LB}(i) = \tau \cdot r_M^{LB}(i-1) + (1-\tau) \cdot r_K(i)$$

$$r_M^*(i) = 0.5 \cdot \left(r_M^{LB}(i) + r_M^{HB}(i) \right) \tag{4.12}$$

with the spectral line index *i* and the notation introduced in equation 4.11.

The iteration starts in the highband at given identification order *N* with

$$r_M^{HB}(N-1) = r_K(N-1) \tag{4.13}$$

and corollary in the lowband

$$r_M^{HB}(0) = r_K(0) \tag{4.14}$$

The result of the recovery process selecting an exponential weight of $\tau = 0.85$ is illustrated in fig. 4.2.5. As compared to fig. 4.2.2 it reveals that the underlying adaptation dynamics in the coherent and the incoherent stimulus case are equal. This is in agreement with the single line filter operation that was examined in section 4.1, where the dynamics also solidified to be independent of the modulation frequency.

Comparison of the ASA filter to the Fast Fourier Transformation

To close the answer on the question, whether the adaptive filter approach to spectrum analysis is methodically favorable we have to contrast our new knowledge to the standard. The Fast Fourier Transformation is one of the most popular and probably one of the most powerful DSP algorithms known [SMI99]. It is designed to compute the spectral components that constitute a given time series featuring a very efficient and elegant numerical strategy [CT65]. But with respect to online observation of time varying spectra the algorithm has two bottlenecks. First it is tailored for post processing time domain data. The time series has to be fully captured before the computations may start. If one considers the implementation of a delayed sliding window variant the numerical efficiency just drops down. Second the method exclusively supports the analysis of frequency combs starting from 0 Hz and finishing at the sampling frequency of the DSP hardware. The spacing is given by the quotient of the sampling frequency and the length of the time series. To benefit from the computation strategy length must be a power of 2. As the FFT is used to analyze a time series in a narrowed frequency band at specified resolution, the algorithm obviously generates a lot of computational overhead.

We will determine the experimental conditions now, that allow to measure the transfer function of the nanooptical model system by means of a radix–2 FFT within a fidelity that is comparable to the ASA identification. We take the root mean squared error of magnitudes and phasing as an indicator of merit. After that we quantify the numerical overhead relative to the ASA filter computations in case of a sliding window implementation. The discussion is open :

1. The coherent stimulus scenario is chosen. Phasing is valid only in that case.
2. The frequency spacing shall be 1 Hz. Thus the sampling frequency and the FFT length must be equal. Length must be a power of 2.
3. Since the system is probed up to 2048 Hz according to the Nyquist criterion the sampling frequency must be at least 4096 Hz.
4. Simulation is prepared for the sampling frequencies 4096 , 8192 , 16384 and 32768 Hz. In all cases the spacing of the FFT frequency comb is guaranteed 1 Hz as specified.
5. The stimulus and the model response are computed for 4096 , 8192 , 16384 and 32768 cycles adding white noise and spurs.
6. The transfer spectra are evaluated based on the created time series.

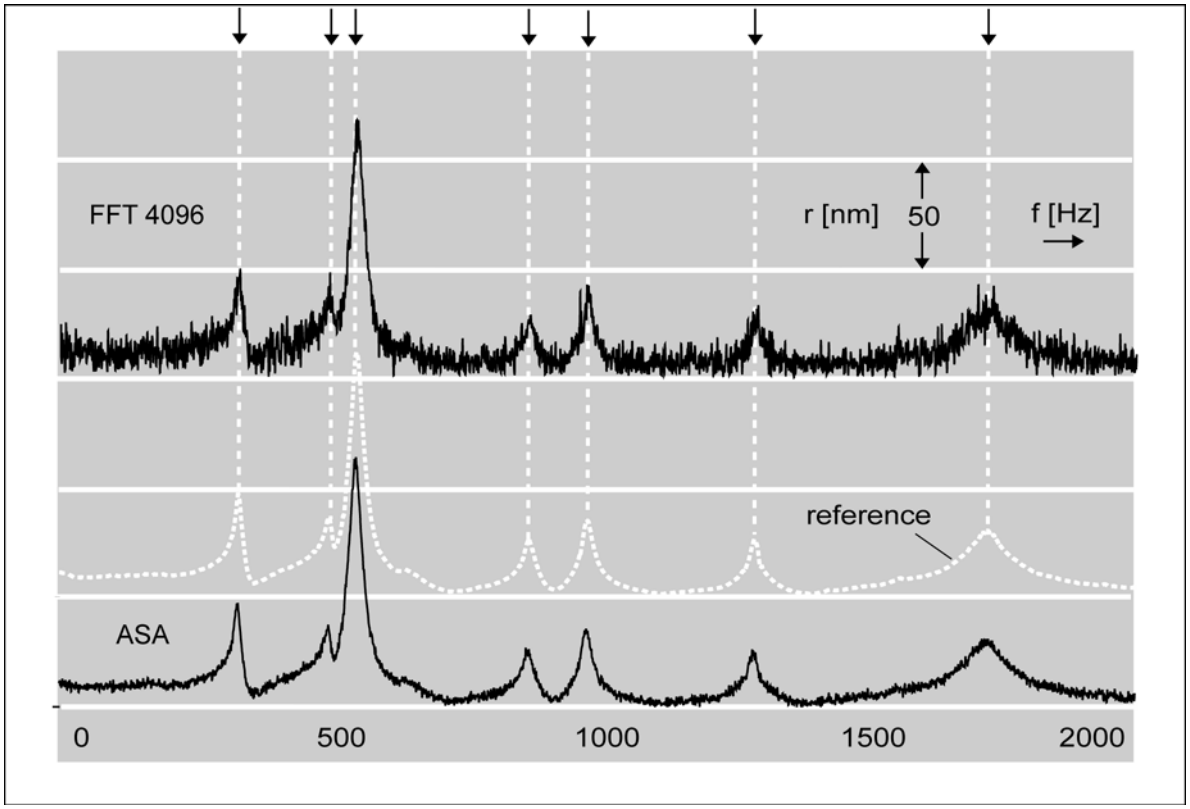

Figure 4.2.6 : *4096 point radix–2 FFT of the piezo actuator model response. Magnitudes are compared with the result of an adaptive spectrum analysis after 1 s adaptation. The recording time of the response time series is also 1 s.*

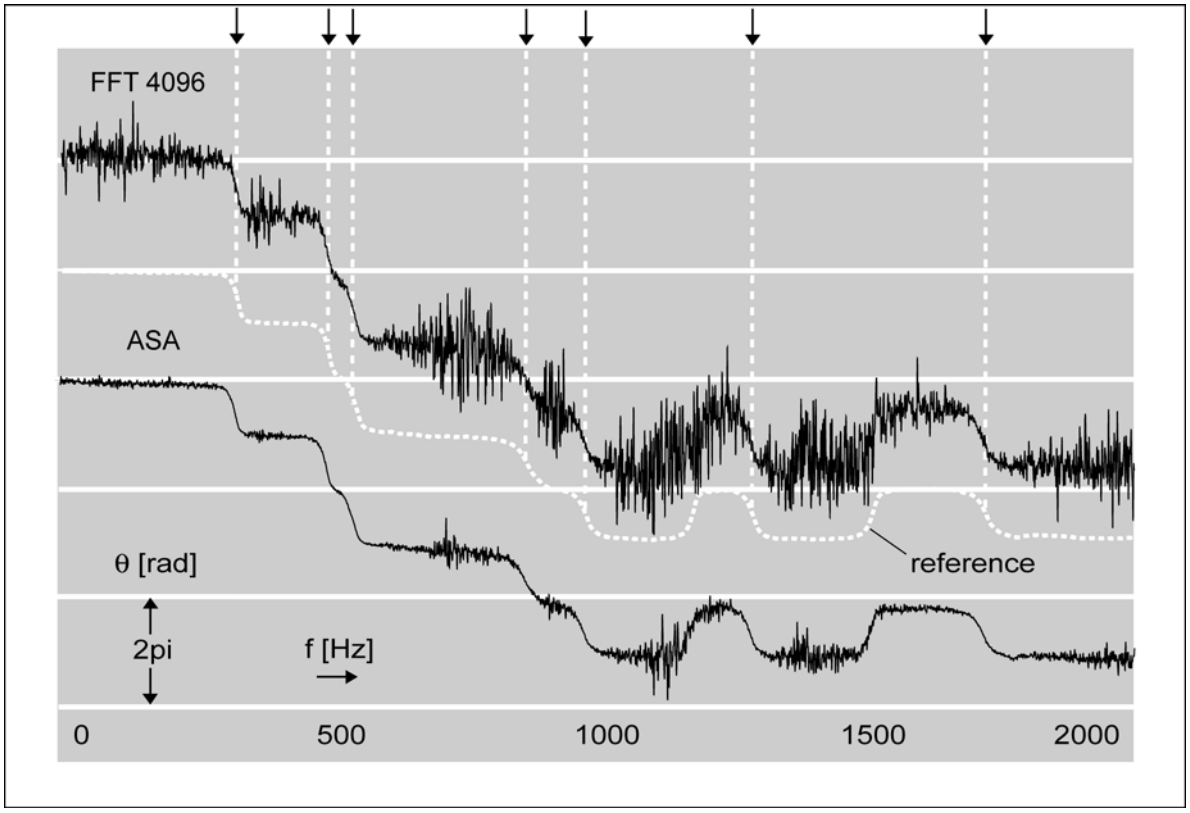

Figure 4.2.6 : *Phasing of the same FFT. Adaptive spectrum analysis data is added for reference. The qualitative course is similar in both techniques, but the noise is significantly reduced in the ASA filter algorithm.*

It is apparent both from magnitude and phase plots, that the signal to noise ratio is significantly higher in the ASA filter data. The 4096 point radix–2 FFT is not competitive. We notice a root mean squared error in the magnitudes of 4.279 and in phasing of 0.847. The reference values from the ASA filter are 0.956 for magnitudes and 0.264 for phasing. It takes a 16384 point radix–2 FFT to measure the transfer function with comparable root mean squared errors in magnitudes and phasing. In that case the values are 1.192 and 0.325. A modern DSP can process the FFT in $N \cdot \log N$ core computation cycles [ANA03]. In our case these are 229376 instruction loops. It has been demonstrated in chapter 3 section 2, that the ASA filter takes 9.5 core instructions per complex oscillator. Since we track 2048 frequencies the effort is 19456 cycles. This is factor 10 less than we pay in the FFT spectrum analysis.

Concerning studies of time varying spectra the answer is crystal clear.

Yes, adaptive spectrum analysis is a very favorable method !